Supplementary Information

Design of V-shaped ionic liquid crystals: their atropisomerization ability and formation of double-gyroid-structured molecular assemblies

Takahiro Ichikawa,[*,a] Soki Obara,[a] Saori Yamaguchi,[a] Yumin Tang,[b] Toshiyo Kato,[c] and Xiangbing Zeng[b]

[a]Department of Biotechnology, Tokyo University of Agriculture and Technology, Naka-cho, Koganei, Tokyo, 184-8588, Japan.
[b]Department of Materials Science and Engineering, University of Sheffield, Sheffield, S1 3JD (UK)
[c]Smart-Core-Facility Promotion Organization, Tokyo University of Agriculture and Technology, Tokyo 184-8588 (Japan)

1. General procedures and materials

General Procedures. ^{1}H-NMR spectra were obtained on a JEOL JNM-ECX500 at 500 MHz and in $CDCl_3$ or DMSO-d_6. Chemical shifts of ^{1}H signals were quoted to $(CH_3)_4Si$ ($\delta = 0.00$) as the internal standard. The thermal properties of the materials were examined with DSC-6000 (Seiko Instruments). The heating and cooling rates were 10 °C min^{-1}. A polarized optical microscope Olympus BX51 equipped with a Linkam hot-stage was used for visual observation. X-ray diffraction measurement was performed using a Rigaku Smart-Lab with CuKα radiation. Synchrotron X-ray diffraction/scattering (XRD) experiments were conducted at beamline *BM28*, *ESRF*. The ionic conductivities were measured with an impedance analyzer Solartron 1260 (frequency range: 10 Hz-10 MHz, applied voltage: 0.4 V). Comb-shaped gold electrodes with a glass substrate were used as a cell for the measurements of ionic conductivity. To determine the cell constant of the cell, a 0.01 mol L^{-1} KCl aqueous solution was employed as a calibration standard.

Materials. All chemical reagents and solvents were obtained from commercial sources and used without purification.

2. Synthesis of [H-Im][TFSI] and [H-Im][FSI]

Scheme S1. Synthesis of [H-Im][TFSI] and [H-Im][FSI].

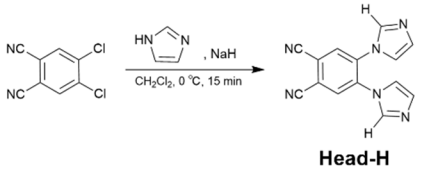

Head-H

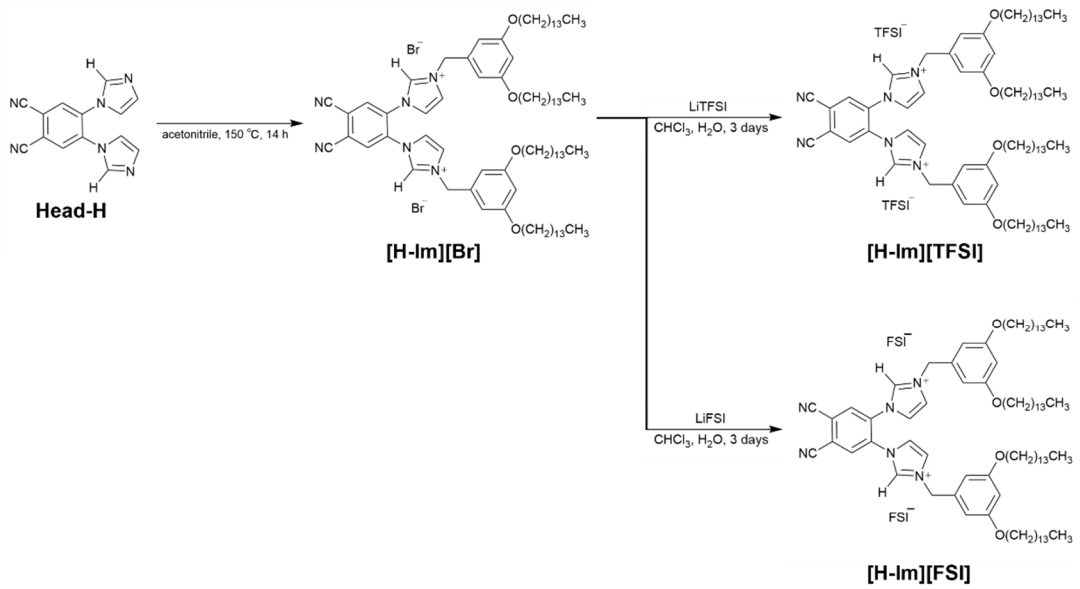

Head-H **[H-Im][Br]** **[H-Im][TFSI]** **[H-Im][FSI]**

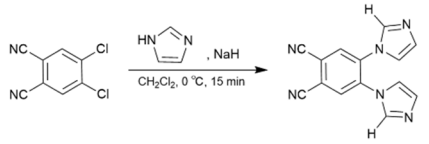

Head-H

Head-H. To 60 % NaH (1.12 g, 37.5 mmol) was added a solution of imidazole (2.59 g, 37.5mmol) in DMF (15 ml) dropwise at 0 ºC. The reaction mixture was stirred for 15 min. A solution of 4,5-dichlorophthalonitrile (1.85 g, 9.36 mmol) in DMF (15 ml) was added and the mixture was stirred for 20 min. Then, NH_4Cl aq. (250 ml) was added to the solution, which yielded a dark green product. The crude product was extracted with ethyl acetate three times. The resulting organic phase was dried over anhydrous $MgSO_4$, filtered, and concentrated under reduced pressure. The crude product was purified by column chromatography on silica gel (eluent: $CHCl_3$/MeOH = 10/1) to afford **Head-H** as a white solid (Yield = 0.83 g, 34%). ^{1}H-NMR (400MHz, DMSO-d_6): δ = 8.60 (s, 2H), 7.67 (s, 2H), 7.07 (s, 2H),7.06 (s, 2H).

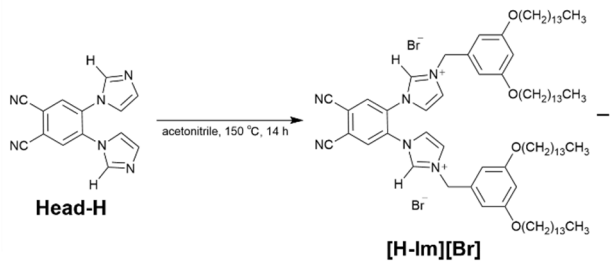

Head-H **[H-Im][Br]**

[H-Im][Br]. An acetonitrile (3 ml) solution of 3,5-bis(tetradecyloxy)benzyl bromide (2.96 g, 5.09 mmol), **Head-H** (0.375 g, 1.44 mmol), and NaI (0.10 g, 0.67 mmol) in a pressure tube equipped with a stirring bar was heated at 150 °C for 14 h with vigorous stirring. The solvent was removed in vacuo. The crude product was used in the next step without further purification.

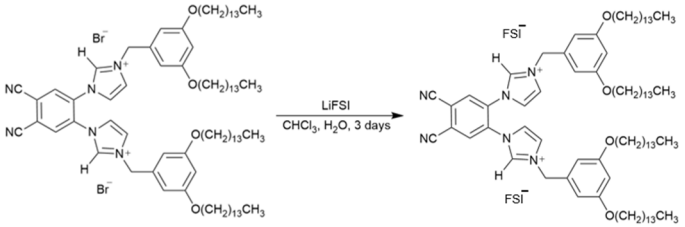

[H-Im][Br] [H-Im][FSI]

[H-Im][FSI]. A solution of **[H-Im][Br]** (0.677 g, 0.466 mmol) and LiFSI (0.637 g, 2.80 mmol) in $CHCl_3$/methanol/water was vigorously stirred at room temperature for 12 h. The reaction mixture was extracted with $CHCl_3$ three times. The resulting organic phase was dried over anhydrous $MgSO_4$, filtered, and concentrated under reduced pressure. The crude product was purified by column chromatography on silica gel (eluent: $CHCl_3$/MeOH = 20/1) to afford **[H-Im][FSI]** as a white solid (yield = 0.116 g, 15%). ^{1}H-NMR (400MHz, DMSO-d_6): δ = 9.66 (s, 2H), 8.86 (s, 2H), 7.88 (s, 2H), 7.83 (s, 2H), 6.55 (s, 2H), 6.50 (s, 2H), 3.91 (m, 8H), 1.66 (m, 8H), 1.41-1.17 (m, 88H), 0.85 (t, J = 5.2Hz, 12H). Elemental analysis calcd. for $C_{84}H_{134}F_4N_8O_{12}S_4$ + $2H_2O$: C, 59.76; H, 8.23; N, 6.64. Found: C, 59.86; H, 8.10; N, 6.08.

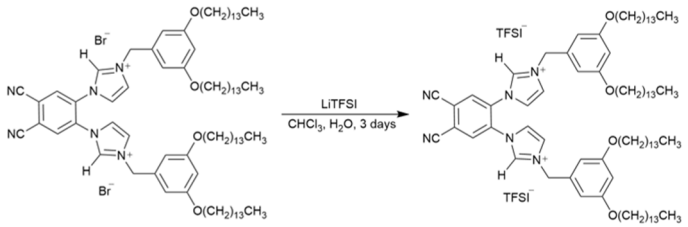

[H-Im][Br] [H-Im][TFSI]

[H-Im][TFSI]. A solution of **[H-Im][Br]** (0.216 g, 0.149 mmol) and LiTFSI (0.256 g, 0.893 mmol) in $CHCl_3$/methanol/water was vigorously stirred at room temperature for 12 h. The reaction mixture was extracted with $CHCl_3$ three times. The resulting organic phase was dried over anhydrous $MgSO_4$, filtered, and concentrated under reduced pressure. The crude product was purified by column chromatography on silica gel (eluent: $CHCl_3$/MeOH = 10/1) to afford **[H-Im][TFSI]** as a white solid (yield = 0.165 g, 60%). ^{1}H-NMR (400MHz, DMSO-d_6): δ = 9.67 (s, 2H), 8.87 (s, 2H), 7.88 (t, J = 2.0 Hz, 4H), 6.31 (t, J = 2H, 1.6Hz), 6,56 (s, 4H), 6.50 (s, 2H), 5.33 (s, 4H), 3.88 (t, J = 6.0 Hz, 8H), 1.66 (m, 8H), 1.41-1.13 (m, 88H), 0.85 (t, J = 6.4 Hz, 12H). ^{13}C-NMR (125MHz, $CDCl_3$): δ = 161.28, 136.73, 133.56, 132.75, 123.84, 123.55, 120.71, 119.93, 118.16, 113.25, 107.31, 102.54, 102.28, 68.37, 54.69, 31.92, 30.11, 29.72, 29.67, 29.60, 29.44, 29.67, 29.17, 26.21, 25.98, 22.68, 14.10. Elemental analysis calcd. for $C_{88}H_{134}F_{12}N_8O_{12}S_4$: C, 57.06; H, 7.29; N, 6.05. Found: C, 57.90; H, 7.59; N, 5.82.

(a)

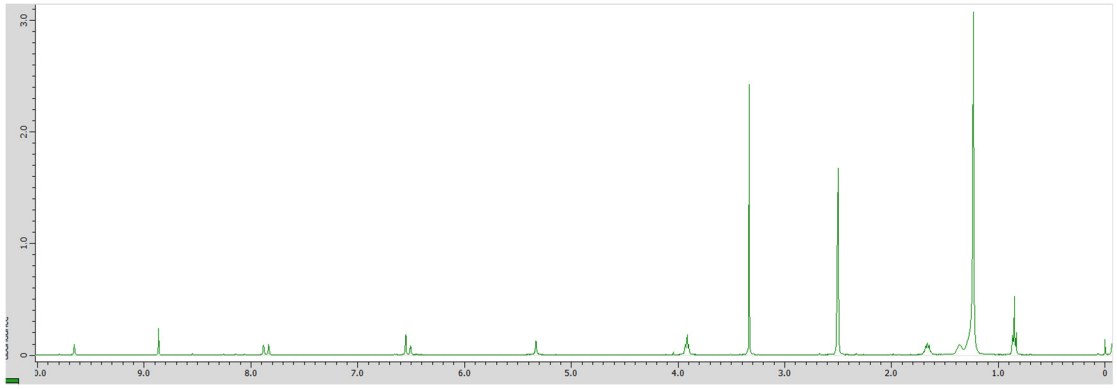

(b)

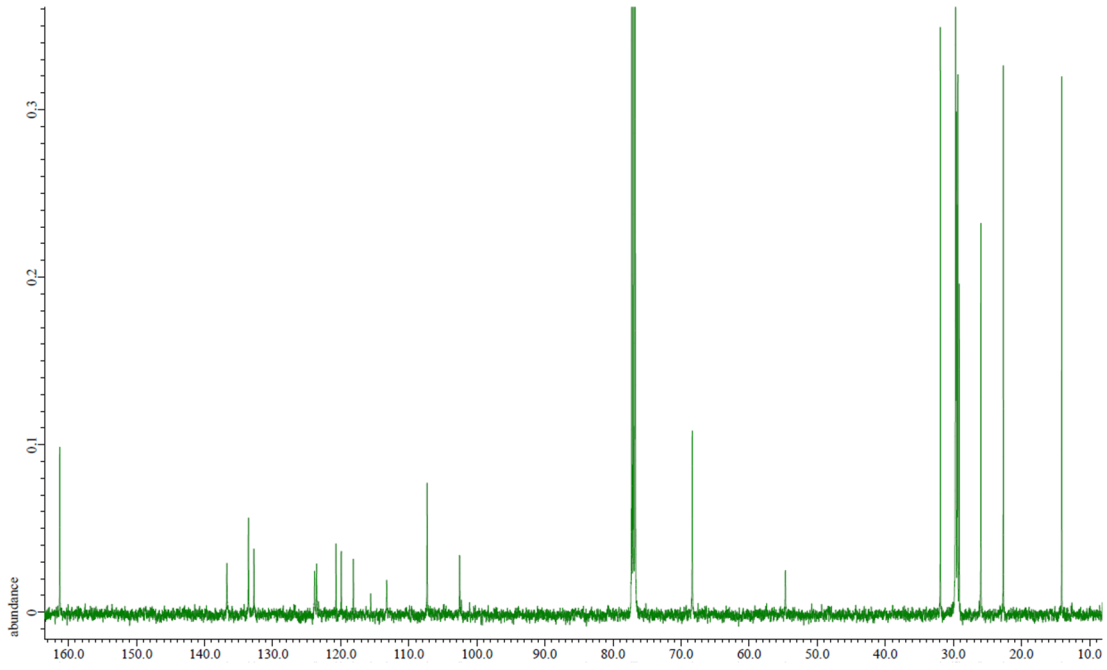

Figure S1. (a) ^{1}H-NMR spectrum of **[H-Im][TFSI]** (DMSO-d_6). (b) ^{13}C-NMR spectrum of **[H-Im][TFSI]** ($CDCl_3$).

3. Synthesis of [Et-Im][TFSI] and [Et-Im][FSI]

Scheme S2. Synthesis of [Et-Im][TFSI] and [Et-Im][FSI].

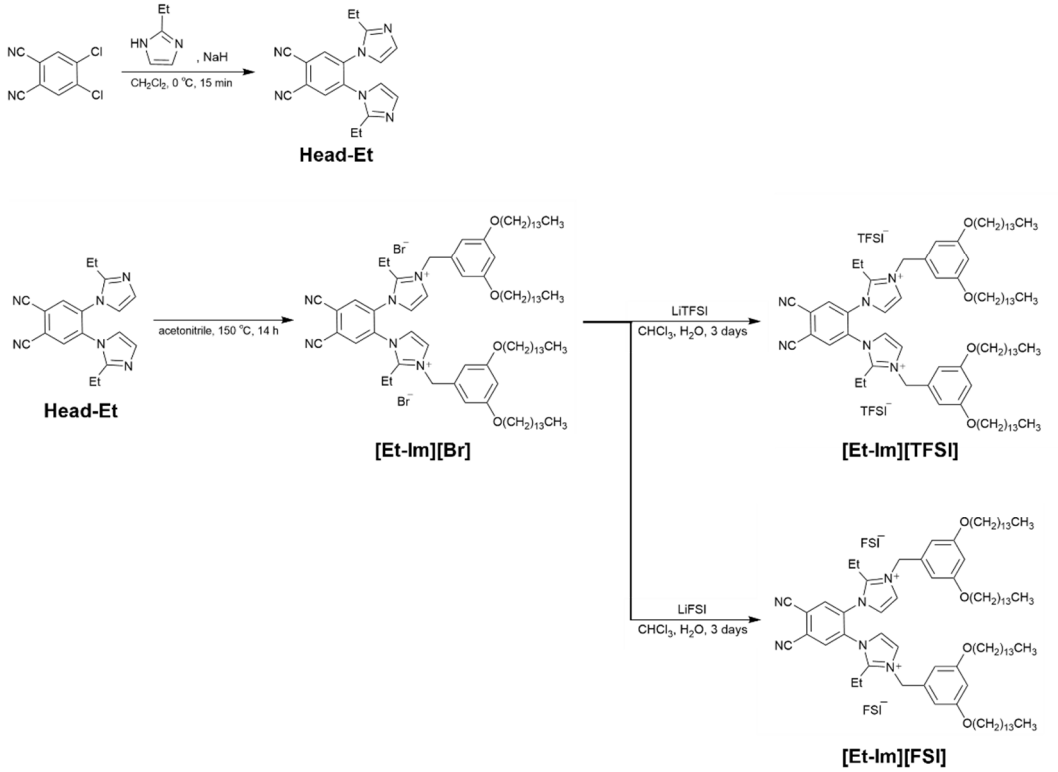

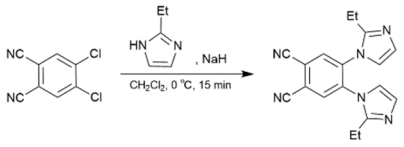

Head-Et

Head-Et. A solution of 2-ethylimidazole (1.95 g, 20.3 mmol) in DMF (15 ml) was dropwised to 60 % NaH (0.370 g, 15.4 mmol) at 0 ºC and stirring for 15 min. A solution of 4,5-dichlorophthalonitrile (1.01 g, 5.13 mmol) in DMF (15 ml) was added and the mixture was stirred for 1 hour at 50 °C. Then, NH_4Cl aq. (250 ml) was added to the solution, which yielded a dark green product. The crude product was extracted with ethyl acetate three times. The resulting organic phase was dried over anhydrous $MgSO_4$, filtered, and concentrated under reduced pressure. The crude product was purified by column chromatography on silica gel (eluent: $CHCl_3$/MeOH = 10/1) to afford **Head-Et** as a white solid (yield = 0.746 g, 46%). ^{1}H-NMR (400MHz, DMSO-d_6): δ = 8.60 (s, 2H), 7.07 (s, 2H), 7.06(s, 2H), 6.87 (s, 4H), 3.77 (m, 4H), 1.09 (t, 6H).

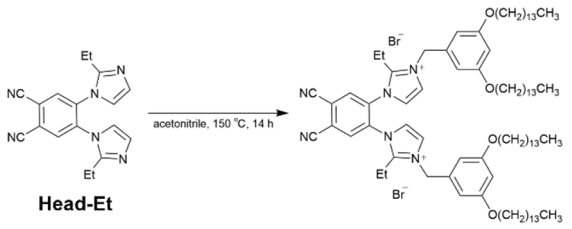

Head-Et **[Et-Im][Br]**

[Et-Im][Br]. An acetonitrile (3 ml) solution of 3,5-bis(tetradecyloxy)benzyl bromide (2.59 g, 4.46 mmol) and **Head-Et** (0.404 g, 1.28 mmol) in a pressure tube equipped with a stirring bar was heated at 150 °C for 14 h with vigorous stirring. The solvent was removed in vacuo. The crude product was used in the next step without further purification.

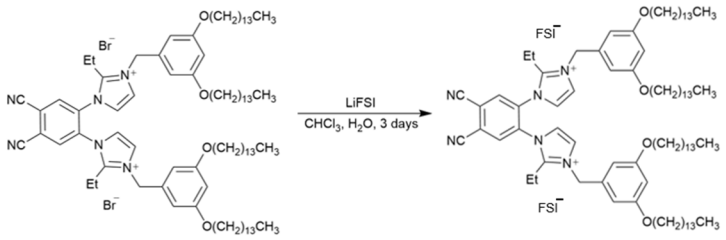

[Et-Im][Br] [Et-Im][FSI]

[Et-Im][FSI]. A solution of **[Et-Im][Br]** (0.187 g, 0.124 mmol) and LiTFSI (0.139 g, 0.744 mmol) in $CHCl_3$/methanol/water was vigorously stirred at room temperature for 3 days. The reaction mixture was extracted with $CHCl_3$ three times. The resulting organic phase was dried over anhydrous $MgSO_4$, filtered, and concentrated under reduced pressure. The crude product was purified by column chromatography on silica gel (eluent: $CHCl_3$/MeOH = 15/1) to afford **[Et-Im][FSI]** as a white solid (yield = 0.0805 g, 38%). ^{1}H-NMR (400MHz, DMSO-d_6) : δ = 9.08-8.96 (2H), 8.0-7.54 (4H), 6.47 (s, 4H), 6.31 (s, 2H), 5.42 (s, 4H), 3.94-3.81 (8H), 3.00 (4H), 1.64 (8H), 1.40-1.16 (88H), 1.12 (6H), 0.85 (t, J = 6.4Hz, 12H). Elemental analysis calcd. for $C_{88}H_{142}F_4N_8O_{12}S_4$ + $2H_2O$: C, 60.59; H, 8.44; N, 6.42. Found: C, 60.93; H, 8.52; N, 5.91.

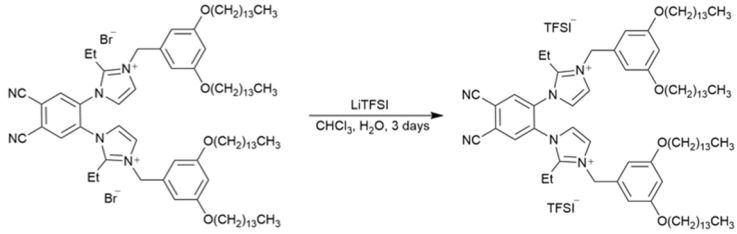

[Et-Im][Br] [Et-Im][TFSI]

[Et-Im][TFSI]. A solution of **[Et-Im][Br]** (0.539 g, 0.357 mmol) and LiTFSI (0.616 g, 2.15 mmol) in $CHCl_3$/methanol/water was vigorously stirred at room temperature for 3 days. The reaction mixture was extracted with $CHCl_3$ three times. The resulting organic phase was dried over anhydrous $MgSO_4$, filtered, and concentrated under reduced pressure. The crude product was purified by column chromatography on silica gel (eluent: $CHCl_3$/MeOH = 15/1) to afford **[Et-Im][TFSI]** as a white solid (yield = 0.348 g, 51%). ^{1}H-NMR (400MHz, DMSO-d_6) : δ = 9.08-8.96 (2H), 8.0-7.54 (4H), 6.47(4H), 6.31(s, 2H), 5.44(s, 4H), 3.88 (t, 8H), 3.20-2.92 (4H), 1.64 (s, 8H), 1.43-1.14 (m, 88H), 1.12 (m, 6H), 0.85 (t, J = 6.8 Hz, 12H). ^{13}C-NMR (125MHz, $CDCl_3$): δ = 161.23, 160.82, 150.43, 135.08, 134.55, 133.21, 132.89, 129.73, 128.89, 124.52, 123.38, 121.72, 121.23, 120.82, 118.57, 118.27, 115.72, 113.40, 106.34, 105.99, 101.97, 101.56, 68.30, 52.86, 32.05, 31.91, 29.70, 29.66, 29.60, 29.41, 29.36, 29.10, 25.93, 22.67, 17.78, 14.88, 14.09, 11.44. Elemental analysis calcd. for $C_{92}H_{142}F_{12}N_8O_{12}S_4$: C, 57.90; H, 7.50; N, 5.87. Found: C, 58.35; H, 7.40; N, 5.82.

(a)

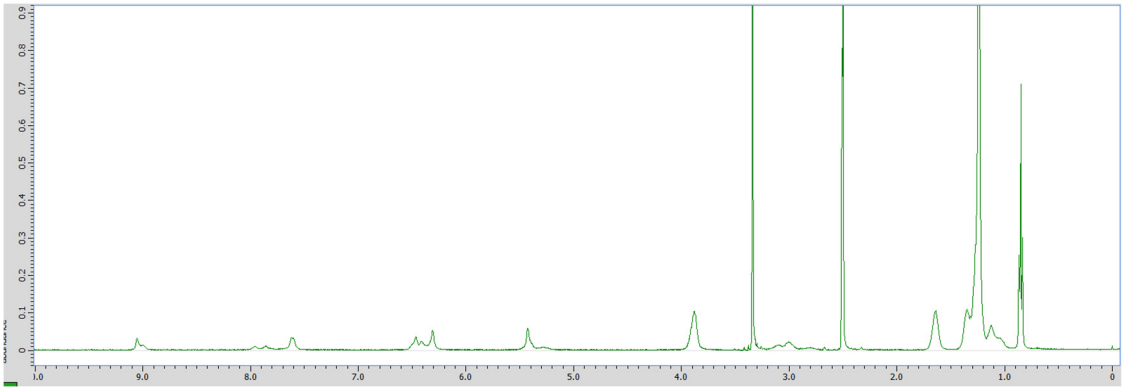

(b)

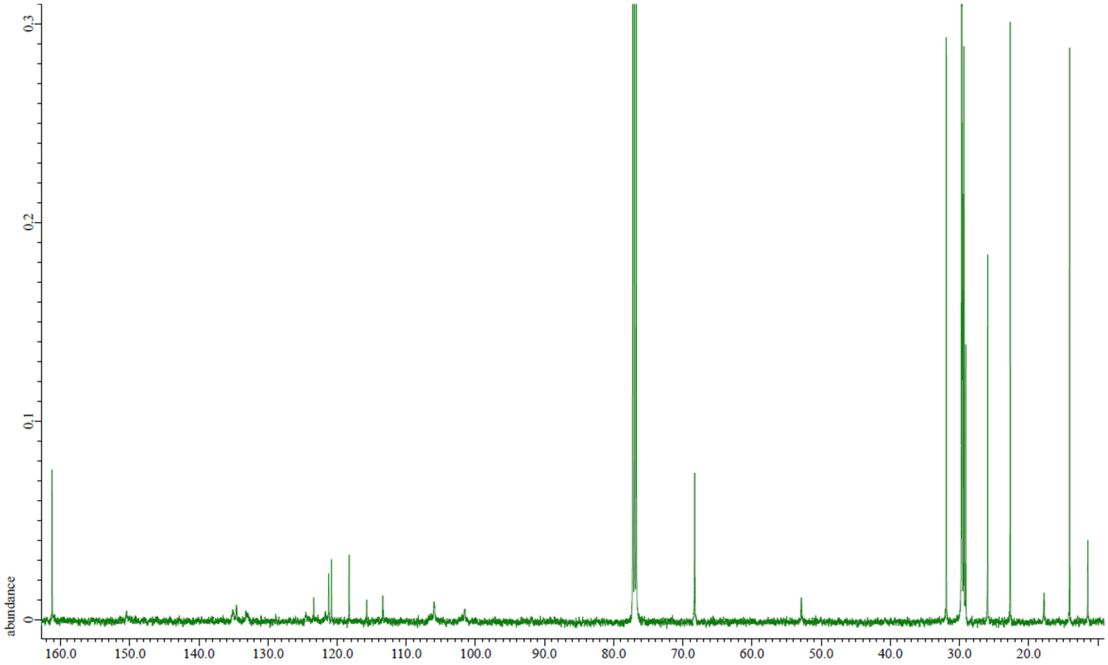

Figure S2. (a) ^{1}H-NMR spectrum of **[Et-Im][TFSI]** (DMSO-d_6). (b) ^{13}C-NMR spectrum of **[Et-Im][TFSI]** ($CDCl_3$).

4. Thermotropic liquid-crystalline behavior of [H-Im][TFSI]

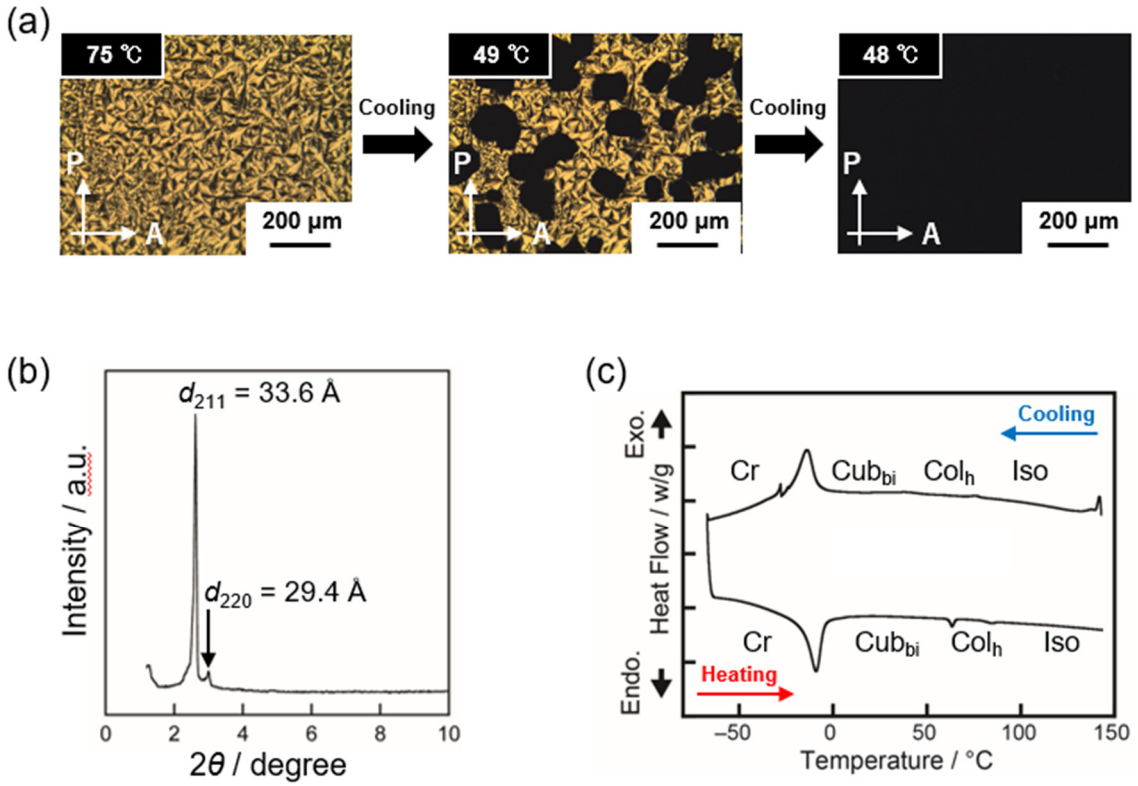

Figure S3. (a) Polarized optical microscopy image of **[H-Im][TFSI]** at various temperatures. (b) XRD pattern of **[H-Im][TFSI]** in the Cub_{bi} phase at 39 °C. (c) DSC thermograms of **[H-Im][TFSI]**.

5. Thermotropic liquid-crystalline behavior of [H-Im][FSI]

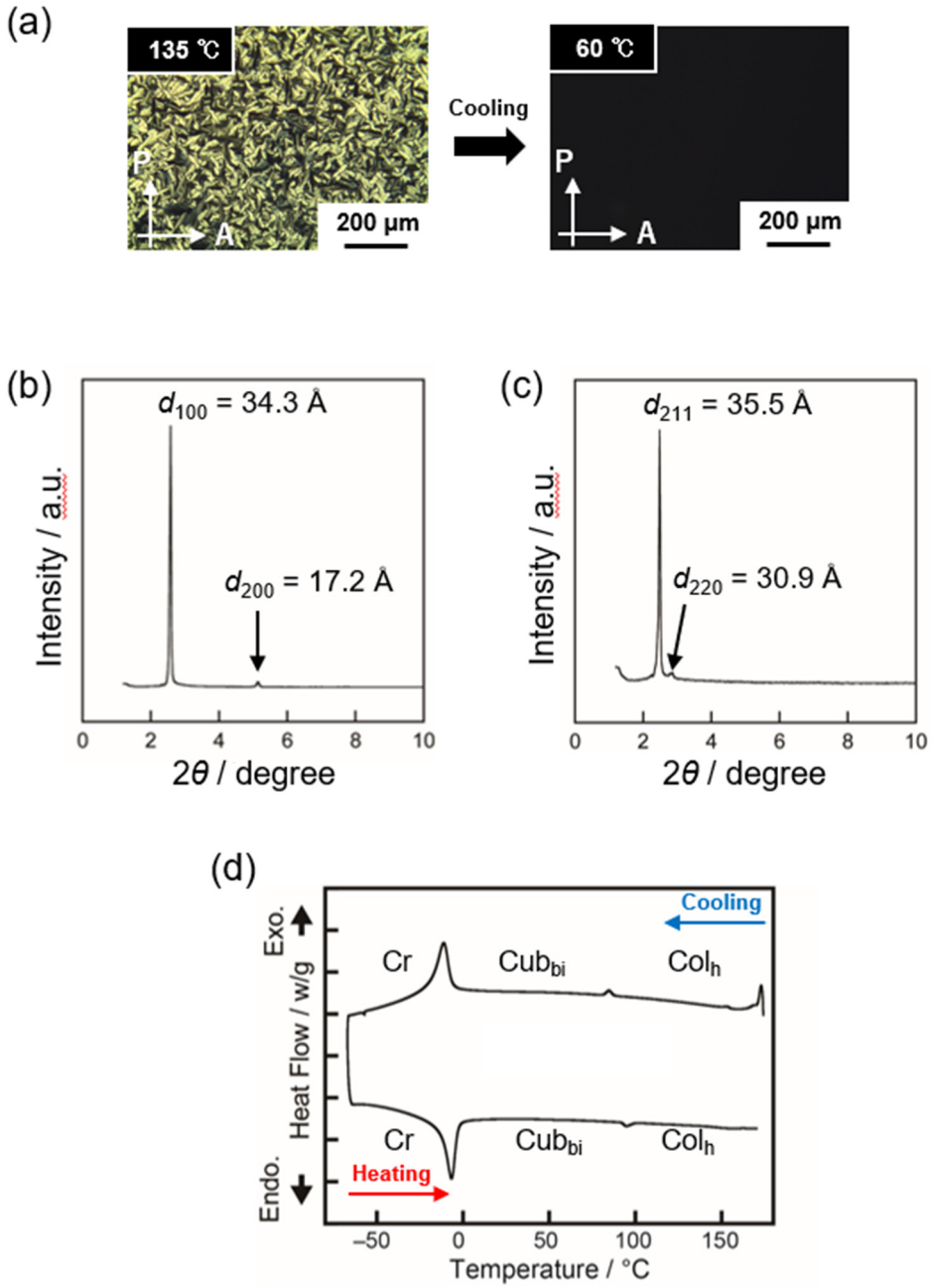

Figure S4. (a) Polarized optical microscopy image of **[H-Im][FSI]** at various temperatures. (b) XRD pattern of **[H-Im][FSI]** in the Col_h phase at 100 °C. (c) XRD pattern of **[H-Im][FSI]** in the Cub_{bi} phase at 80 °C. (d) DSC thermograms of **[H-Im][FSI]**.

6. Thermotropic liquid-crystalline behavior of [Et-Im][TFSI]

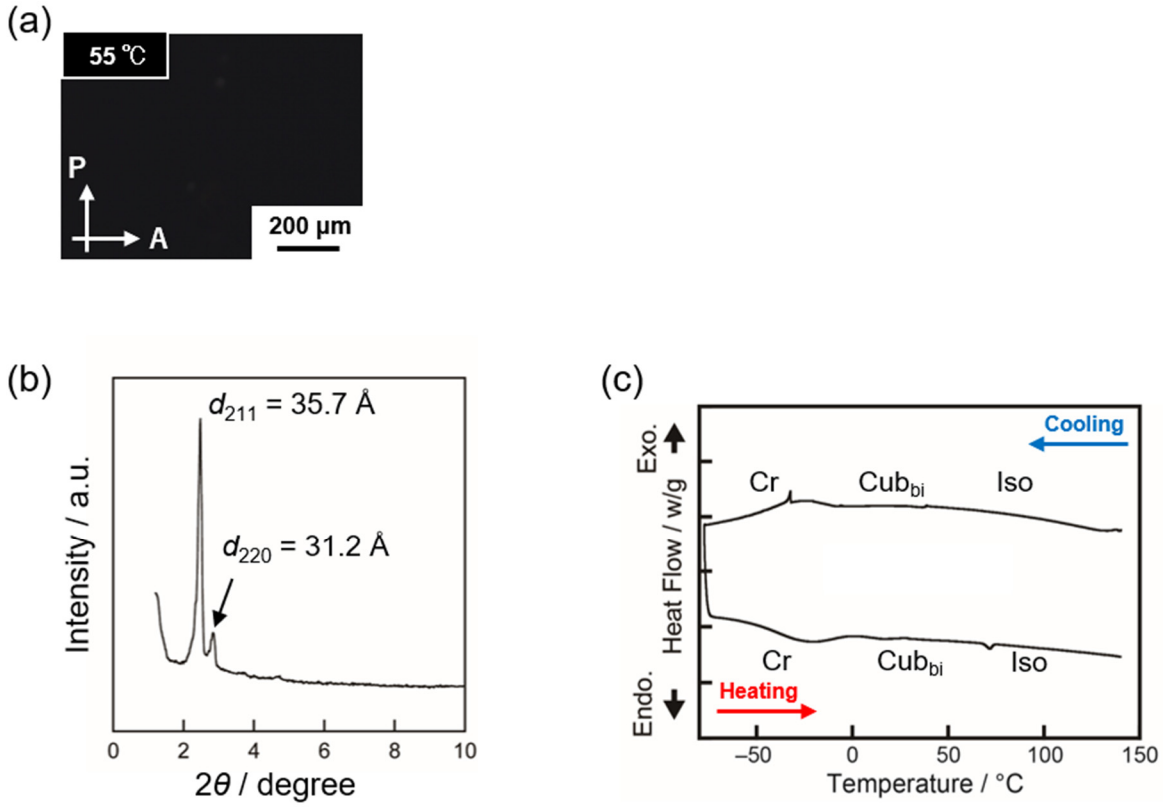

Figure S5. (a) Polarized optical microscopy image of **[Et-Im][TFSI]** at 55 °C in the Cub$_{bi}$ phase. (b) XRD pattern of **[Et-Im][TFSI]** in the Cub$_{bi}$ phase at 48 °C. (c) DSC thermograms of **[Et-Im][TFSI]**.

7. Thermotropic liquid-crystalline behavior of [Et-Im][FSI]

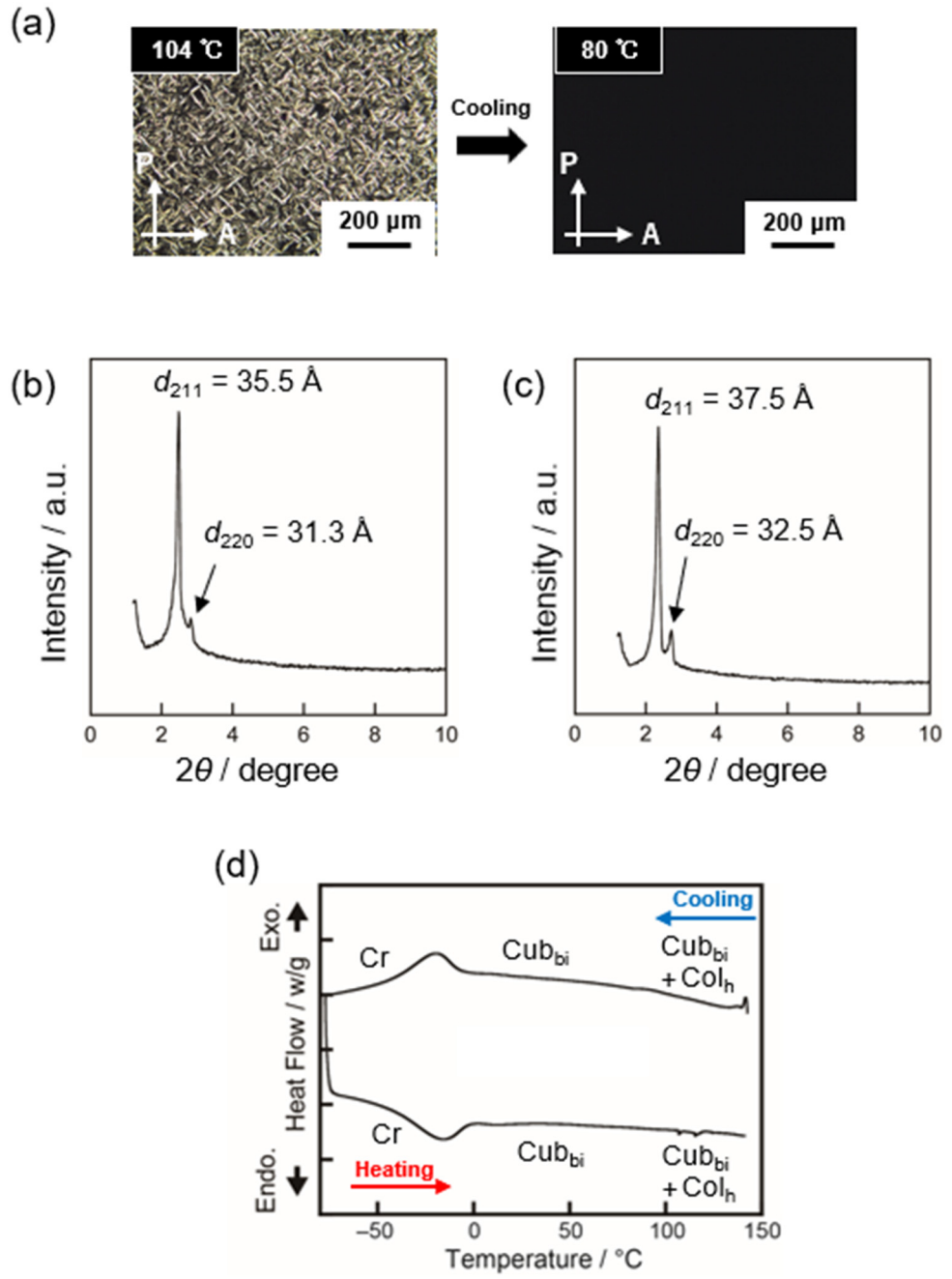

Figure S6. (a) Polarized optical microscopy image of **[Et-Im][FSI]** at various temperatures. (b) XRD pattern of **[Et-Im][FSI]** in a two-phase coexistence state of Col_h and Cub_{bi} phases at 130 °C. (c) XRD pattern of **[Et-Im][FSI]** in the Cub_{bi} phase at 72 °C. (d) DSC thermograms of **[Et-Im][FSI]**.

8. Summary of Phase Transition Behaviour

Table S1. Thermal Properties of **[H-Im][X]**, **[Me-Im][X]**, and **[Et-Im][X]**

Compound	Phase Transition temperature on cooling[a]						
[H-Im][TFSI]	Iso	93 (0.11)	Col_h	49 (0.33)	Cub_{bi}	−3 (12.8)	Cr
[H-Im][FSI]	Iso	156 (0.17)	Col_h	90 (0.58)	Cub_{bi}	1 (18.5)	Cr
[Me-Im][TFSI]	Iso	130[c] (-[b])	Col_h	78 (0.70)	Cub_{bi}	0 (6.6)	Cr
[Me-Im][FSI]	Iso	-[b] (-[b])	Col_h	110 (0.78)	Cub_{bi}	5 (12.4)	Cr
[Et-Im][TFSI]	Iso	71[c] (-[b])	Cub_{bi}	−2 (14.5)	Cr		
[Et-Im][FSI]	Iso	126[c] (-[b])	Col_h + Cub_{bi}	116[c] (-[b])	Cub_{bi}	0 (16.8)	Cr

[a)]Phase transition temperatures (°C) and enthalpies of transition (mJ/mg, in parentheses) determined by DSC on the cooling rates of 10 °C min^{-1}. Transition temperatures of some broad peaks were taken at the onset points of the transition peaks. Cr: crystalline; Col_h: hexagonal columnar; Cub_{bi}: bicontinuous cubic, Iso: isotropic. [b)]Not detected by DSC. [c)]Phase transition temperature was determined by polarized optical microscopic observation.

9. Analysis of Nanostructures

9. 1. Synchrotron XRD measurement

Synchrotron XRD diffractograms of **[H-Im][TFSI]** are shown in **Figure S7** to have two phase transitions (displayed in green) on the first heating process from 30 ℃ (Cry, Crystalline phase). Crystalline compound **[H-Im][TFSI]** was observed to melt into the first LC phases from the phase transition at around 54 ℃. This LC phase can be indexed as a bicontinuous cubic phase with $Ia\bar{3}d$ symmetry (Cub_{bi} / $Ia\bar{3}d$), featuring two intensive Bragg reflections (*211*) and (*220*), labelled in blue. This LC phase then transitioned into a second LC phase from the phase transition at around 69 ℃. The second LC phase can be indexed into a hexagonal columnar phase (Col_h) with the q-vector values of its Bragg peaks in red in a ratio of $1:\sqrt{3}:2$.

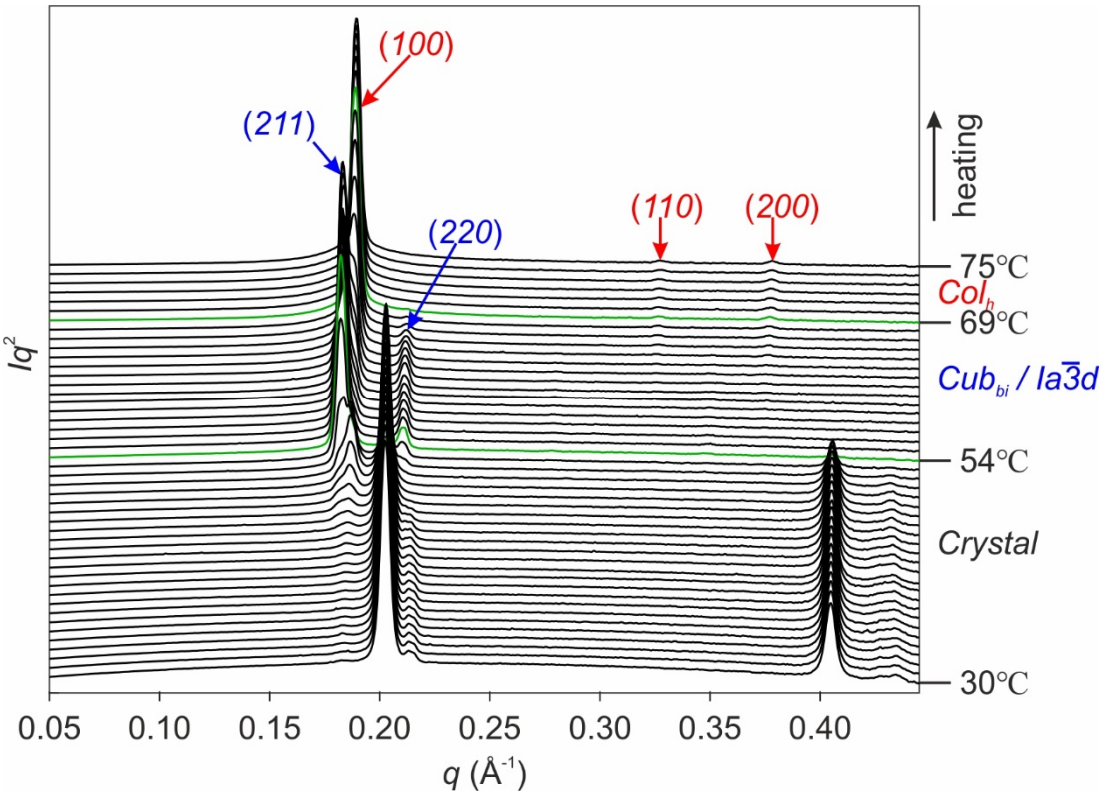

Figure S7. Powder SAXS diffractograms of phases formed in **[H-Im][TFSI]**, recorded on first heating from 30 (Crystal) to 75 ℃ (Col_h) with a rate of 2 ℃/min.

Reversibly, on the first cooling process, this Col_h phase started to convert to Cub_{bi} / $Ia\bar{3}d$ phase at a relatively lower temperature of 59 °C. This is displayed in **Figure S8a** and **8b**.

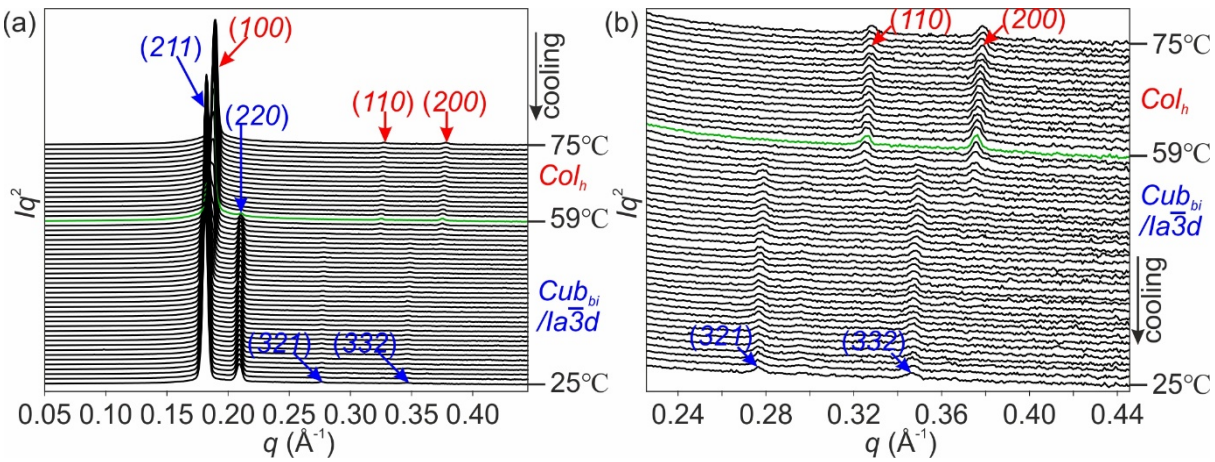

Figure S8. (a) Powder SAXS diffractograms of phases emerged in **[H-Im][TFSI]** recorded on first cooling from 75 to 45 °C with a rate of 2 °C/min. (b) SAXS diffractograms with expanded scale in (a) to show clearly the weaker peaks.

While, on further heating from 60 °C, this Col_h phase gradually transitioned to isotropic (Iso) at 105 °C, as shown in **Figure S9**.

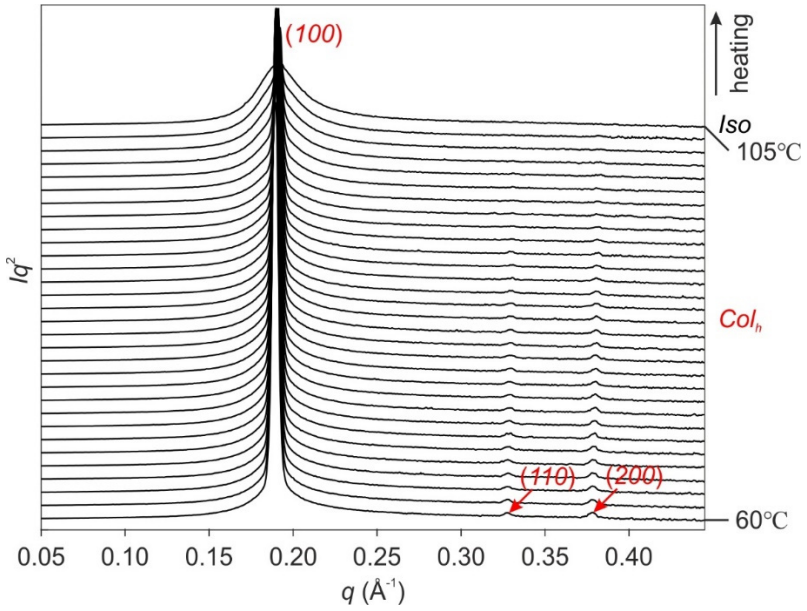

Figure S9. Powder SAXS diffractograms of phases formed in **[H-Im][TFSI]** recorded on heating from 60 to 105 °C with a rate of 2 °C/min.

Moreover, on cooling from 105 °C (Iso), this Col_h phase formed at 103 °C, as shown in **Figure S10**.

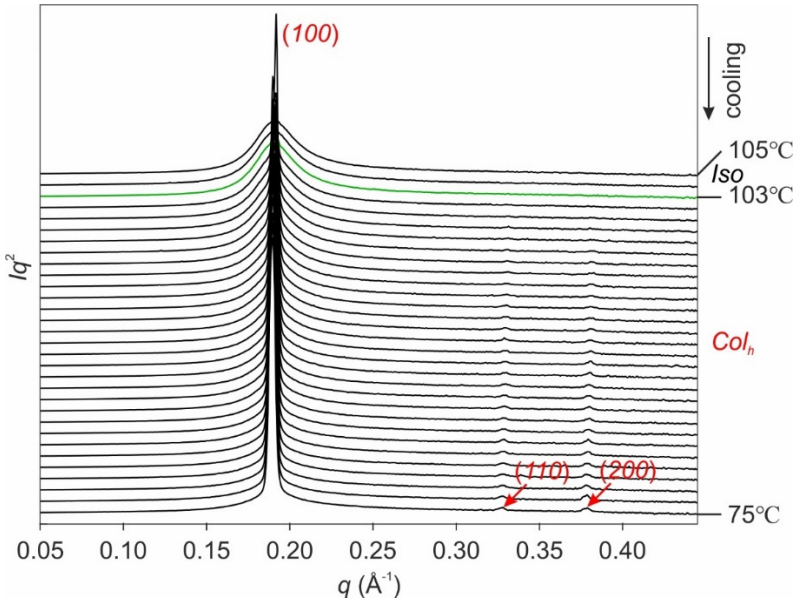

Figure S10. Powder SAXS diffractograms of phases formed in **[H-Im][TFSI]** recorded on cooling from 105 to 75 °C with a rate of 2 °C/min.

As for the **[Et-Im][TFSI]** compound, on the first heating process from 30 °C (Cry), Cub_{bi} / $Ia\bar{3}d$ phase emerged at 45 °C, as shown in **Figure S11**.

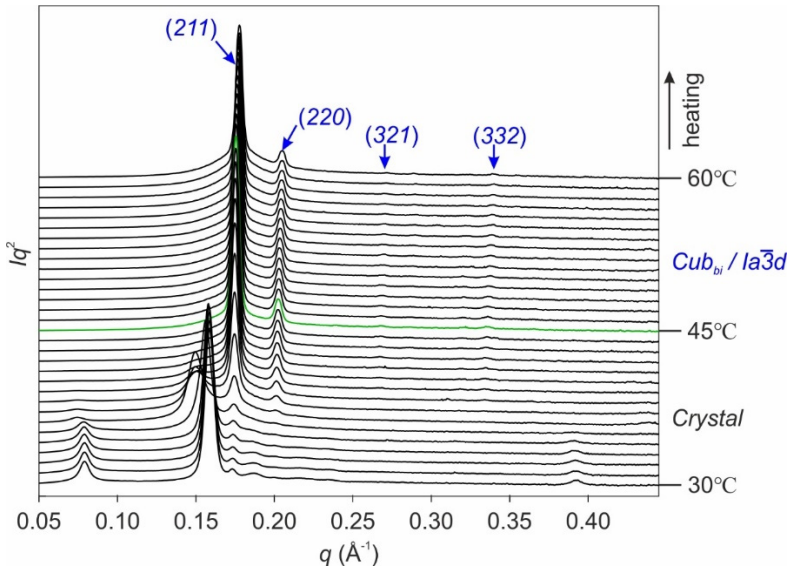

Figure S11. Powder SAXS diffractograms of phases formed in **[Et-Im][TFSI]** recorded on first heating from 30 to 60 °C with a rate of 2 °C/min.

While, on the first cooling from 60 °C, this Cub_{bi} / $Ia\bar{3}d$ phase converted to Cry phase at 36 °C, as displayed in **Figure S12**.

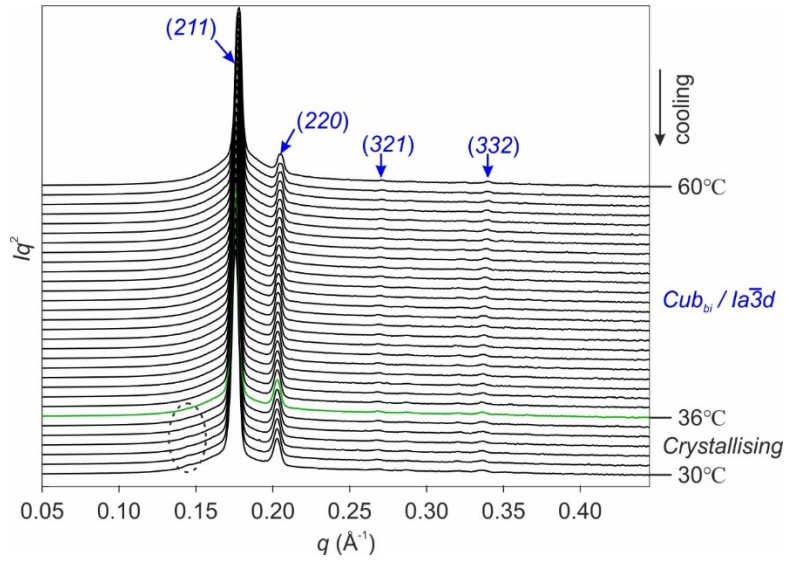

Figure S12. Powder SAXS diffractograms of phases formed in **[Et-Im][TFSI]** recorded on first cooling from 60 to 30 °C with a rate of 2 °C/min.

Notably, on further heating from 60 °C, this Cub_{bi} / $Ia\bar{3}d$ phase transitioned directly into *Iso* phase at 71 °C, without an intermediate Col_h phase as the case in **[H-Im][TFSI]** compound. This is shown in **Figure S13**.

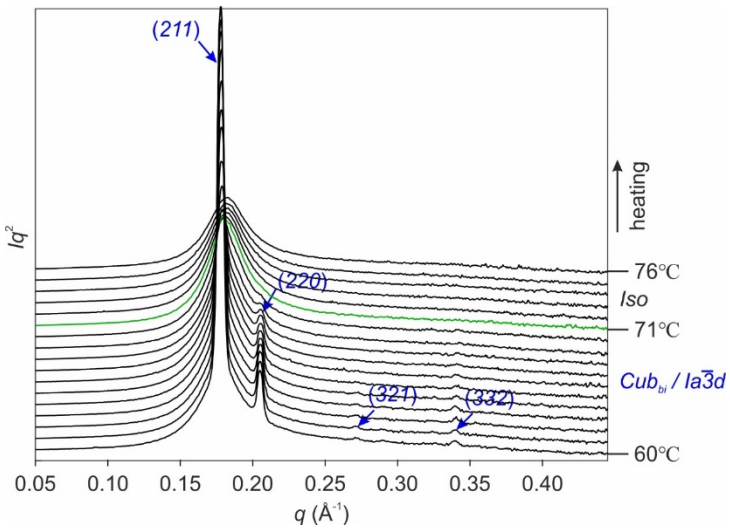

Figure S13. Powder *SAXS* diffractograms of phases formed in **[Et-Im][TFSI]** compound, recorded on heating from 60 to 76 °C with a rate of 2 °C/min.

Interestingly, on cooling from 75 °C, Iso phase would stay to a relatively low temperature (as observed here, to 30 °C), with its broad diffuse peak shifting to a small *q*-vector value. This is shown in **Figure S14**.

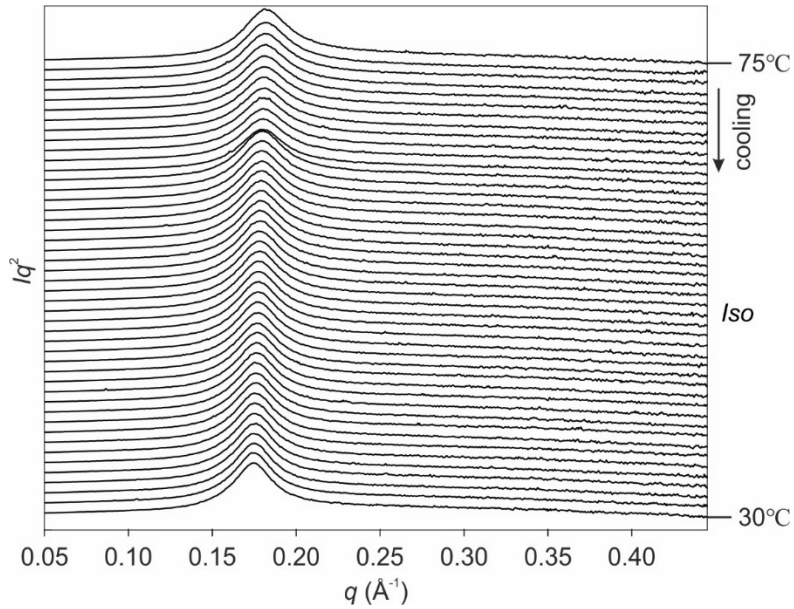

Figure S14. Powder *SAXS* diffractograms of the *Iso* developed in **[Et-Im][TFSI]** recorded on cooling from 75 to 30 °C with a rate of 2 °C/min.

9. 2. Reconstruction of electron density map

Firstly, the index on this Col_h phase is indicated in **Figure S15** with details summarised in **Table S2**.

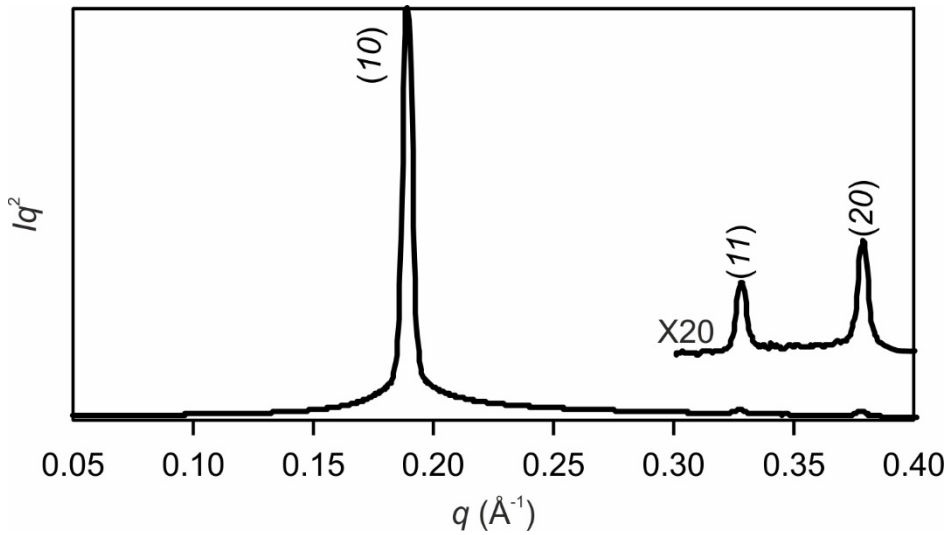

Figure S15. Powder SAXS diffractograms of the Col_h phase in **[H-Im][TFSI]** recorded at 75 ℃ on heating from 30 to 75 ℃ with a rate of 2 ℃/min.

Table S2. Index, experimental and calculated *d*-spacing, intensity (Lorentz and Multiplicity corrected, and normalised to the strongest (*10*) peak), and the corresponding calculated lattice parameters of the *Col*$_h$ phase formed in **[H-Im][TFSI]** at 75 ℃ on heating from 30 ℃.

Phase: Col_h					
(*hkl*)	$d_{exp.}$ (Å)	$d_{calc.}$ (Å)	Intensity	Multiplicity	Phase
(*10*)	33.19	33.21	100	6	0
(*11*)	19.18	19.17	0.89	6	π
(*20*)	16.61	16.60	1.49	6	π
Lattice parameter: a = 38.35 Å					

The two-dimensional ρ-map of this Col_h phase is then reconstructed based on the intensity, multiplicity, and a selected phase combination of the peaks in **Table S2**, as shown in **Figure S16**.

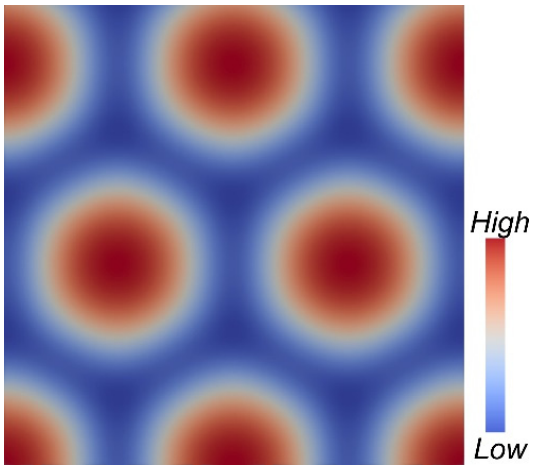

Figure S16. Two-dimensional ρ-map of the Col_h phase in **[H-Im][TFSI]** compound at 75 °C, reconstructed by using the data listed in **Table S2**. Moreover, the structural data of this Col_h phase is calculated to help understand the molecular arrangement, and is summarised in **Table S3**.

Table S3. Structural data of the Col_h phase in **[H-Im][TFSI]** at 75°C.[a]

Phase	a, b (nm)	V_{cell} (nm^3)	V_{mol} (nm^3)	n_{cell}
Col_h	3.8	7.1	2.4	2.9

[a] Abbreviations: $V_{cell} = a^2\, h\, sin(60°)$, the volume of the unit cell; h is the thickness of each molecular raft, here is estimated to be 0.56 nm (more details refer to **Table S6**); V_{mol} is the molecular volume, calculated according to the crystal volume increments by Immirzi;[1] $n_{cell} = V_{cell} / V_{mol}$, is the number of molecule in each cell with h thickness.

To gain an insight into the molecular self-assembly in the Cub_{bi} / $Ia\bar{3}d$ phase in **[H-Im][TFSI]**, the Cub_{bi} / $Ia\bar{3}d$ phase is indexed in detail as shown in **Figure S17** and **Table S4**.

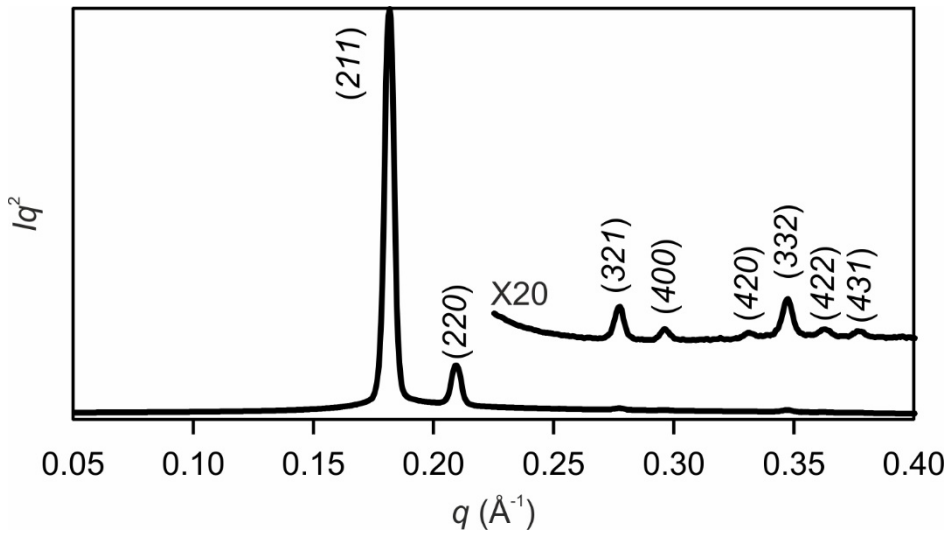

Figure S17. Powder SAXS diffractograms of the Cub_{bi} / $Ia\bar{3}d$ phase in **[H-Im][TFSI]** recorded at 45 °C on cooling from 75 to 45 °C with a rate of 2 °C/min.

Table S4. Index, experimental and calculated *d*-spacing, intensity (Lorentz and Multiplicity corrected, and normalised to the strongest (*211*) peak), and the corresponding calculated lattice parameters of the Cub_{bi} / $Ia\bar{3}d$ phase formed in **[H-Im][TFSI]** at 45 °C on cooling from 75 °C (Col_h).

Phase: Cub_{bi} / $Ia\bar{3}d$					
(*hkl*)	$d_{exp.}$ (Å)	$d_{calc.}$ (Å)	Intensity	Multiplicity	Phase
(*211*)	34.60	34.64	100	24	π
(*220*)	29.99	29.97	19.08	12	π
(*321*)	22.66	22.67	0.19	48	0
(*400*)	21.21	21.20	0.44	6	0
(*420*)	18.98	18.97	0.05	24	0
(*332*)	18.10	18.10	0.47	24	π
(*422*)	17.31	17.32	0.08	24	0
(*431*)	16.66	16.64	0.03	48	π
Lattice parameter: a = 84.84 Å					

With the intensity, multiplicity listed in **Table S4**, three-dimensional ρ-map of the Cub_{bi} / $Ia\bar{3}d$ phase in **[H-Im][TFSI]** compound is further reconstructed with a phase combination selected (as shown in **Table S4**), as shown in **Figure S18**.

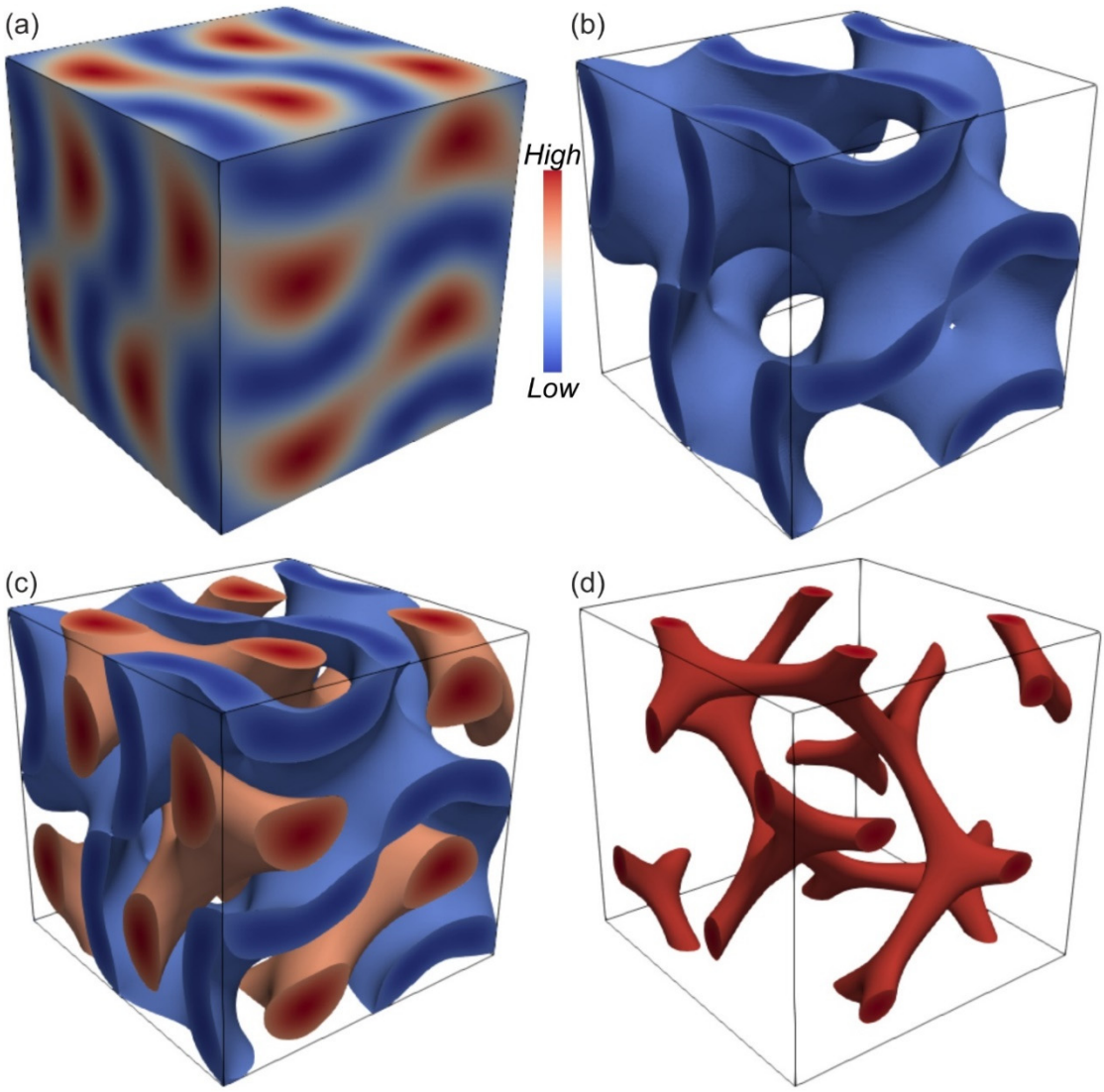

Figure S18. Three-dimensional ρ-map of the Cub_{bi} / $Ia\bar{3}d$ phase in **[H-Im][TFSI]** at 45 °C, reconstructed by using the data listed in **Table S4**. (a) Isoelectron surface of the unit cell of the Cub_{bi} / $Ia\bar{3}d$ phase, showing the continuous network of the relatively high-ρ region in red and the intermediate continuum of the relatively low-ρ region in blue. (b) Isoelectron surface enclosing the lowest 30% unit cell volume, showing the distribution of the flexible aliphatic chains at the triply periodic minimum surface (TPMS). (c) The isoelectron surface in orange and isoelectron surface in blue enclose the highest 20% and lowest 30% unit cell volume, respectively. (d) The isoelectron surface in red shows the very high-ρ region (highest 5%) to visualise the two continuous networks formed by the aromatic/ionic building blocks.

Similarly, the Cub_{bi} / $Ia\bar{3}d$ phase in **[Et-Im][TFSI]** compound is indexed in detail as shown in **Figure S19** and **Table S5**.

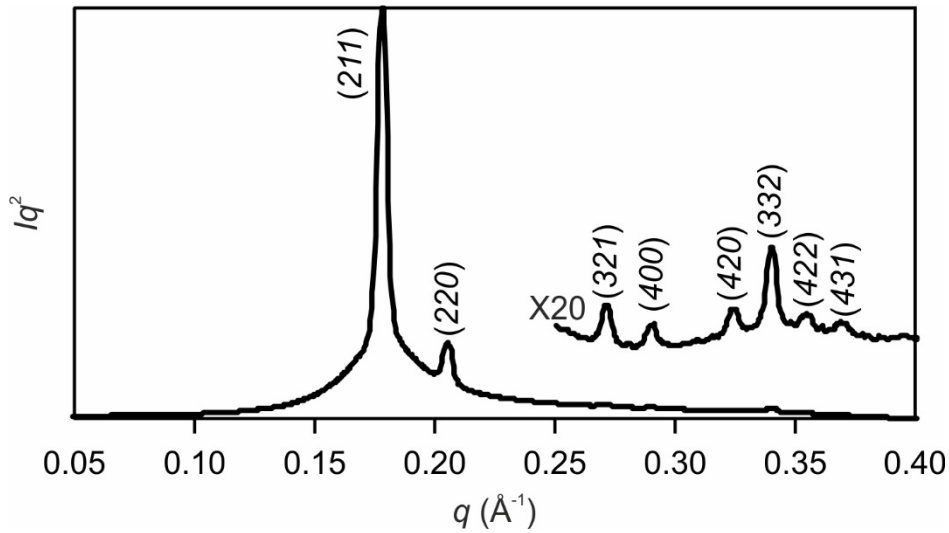

Figure S19. Powder *SAXS* diffractogram of the Cub_{bi} / $Ia\bar{3}d$ phase in **[Et-Im][TFSI]** compound, recorded at 60 ℃ on heating from 30 to 60 ℃ with a rate of 2 ℃/min.

Table S5. Index, experimental and calculated d-spacing, intensity (Lorentz and Multiplicity corrected, and normalised to the strongest (*211*) peak), and the corresponding calculated lattice parameters of the Cub_{bi} / $Ia\bar{3}d$ phase formed in **[Et-Im][TFSI]** compound at 60 ℃ on heating from 30 ℃ (*Crystal*).

Phase: Cub_{bi} / $Ia\bar{3}d$					
(*hkl*)	$d_{exp.}$ (Å)	$d_{calc.}$ (Å)	Intensity	Multiplicity	Phase
(*211*)	35.38	35.59	100	24	π
(*220*)	30.65	30.64	17.96	12	π
(*321*)	23.19	23.17	0.23	48	0
(*400*)	21.69	21.67	1.00	6	0
(*420*)	19.41	19.40	0.33	24	0
(*332*)	18.50	18.50	1.09	24	π
(*422*)	17.73	17.71	0.17	24	0
(*431*)	17.02	17.03	0.07	48	π
Lattice parameter: a = 87.18 Å					

With the intensity, multiplicity listed in **Table S5**, three-dimensional ρ-map of the Cub_{bi} / $Ia\bar{3}d$ phase in **[Et-Im][TFSI]** compound is also reconstructed with the same phase combination selected as in the case of **[H-Im][TFSI]** compound, as shown in **Figure S20**.

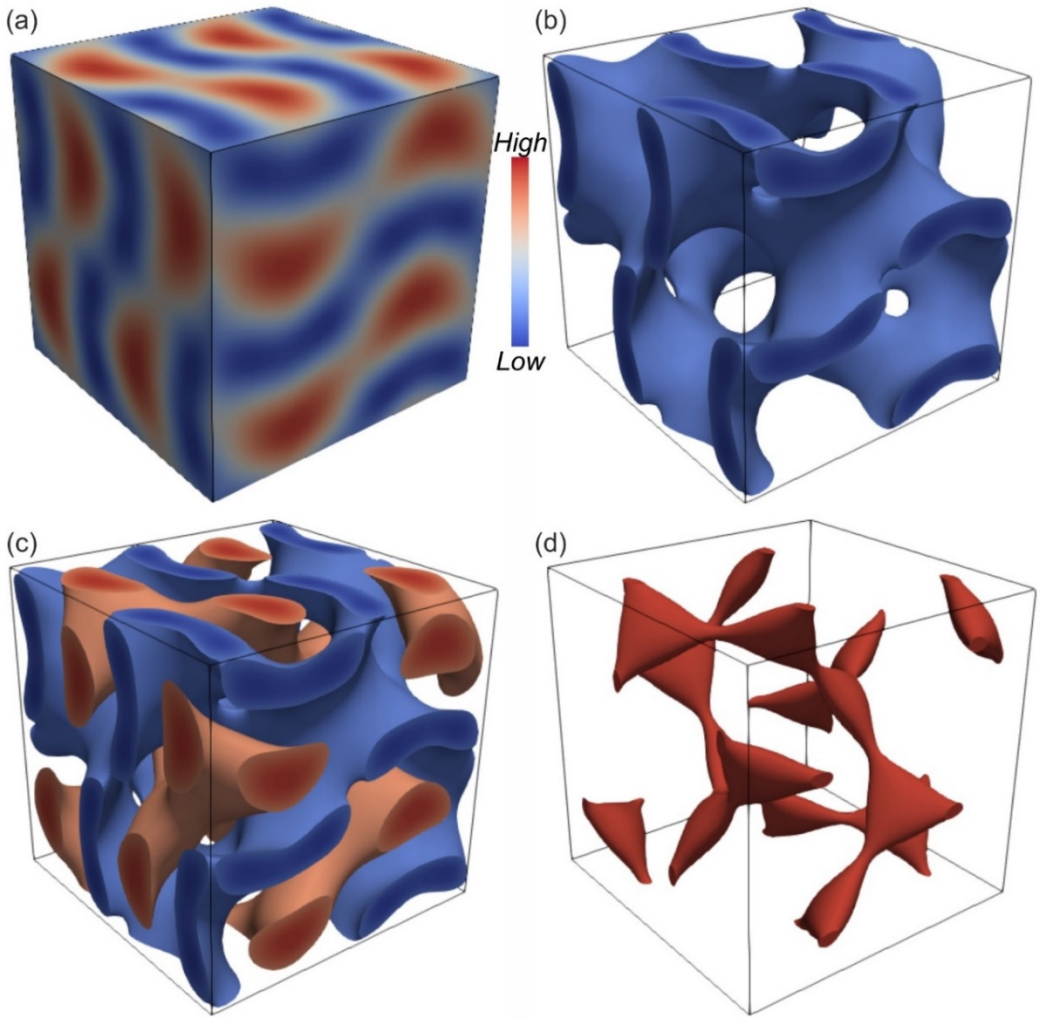

Figure S20. Three-dimensional ρ-map of the Cub_{bi} / $Ia\bar{3}d$ phase in **[Et-Im][TFSI]** at 60 ℃, reconstructed by using the data listed in **Table S5**. (a) Isoelectron surface of the unit cell of the Cub_{bi} / $Ia\bar{3}d$ phase, showing the continuous network of the relatively high-ρ region in red and the intermediate continuum of the relatively low-ρ region in blue. Notably, holes are seen to as approaching close to the TPMS**.** (b) Isoelectron surface enclosing the lowest 30% unit cell volume, showing the distribution of the flexible aliphatic chains at TPMS. (c) The isoelectron surface in orange and isoelectron surface in blue enclose the highest 20 % and lowest 30% unit cell volume, respectively. (d) The isoelectron surface in red shows the very high-ρ region (highest 5%) to visualise the two continuous networks formed by the aromatic/ionic building blocks. The junction area is seen to be more triangular-like.

9. 3. Comparison of electron density maps

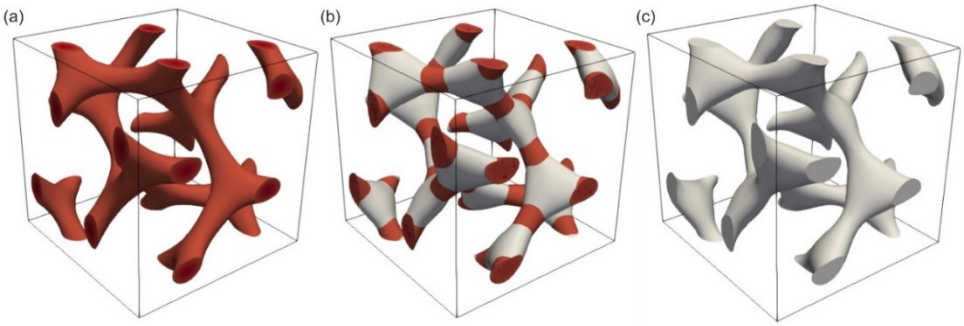

Figure S21. Comparison of the high-ρ region of the Cub_{bi} / $Ia\bar{3}d$ phase formed in **[H-Im][TFSI]** and **[Et-Im][TFSI]**. (a) Isoelectron surface in red enclosing the highest 10% unit cell volume, showing the cylinder-like segments in the bicontinuous networks. (b) Combination of the high-ρ region of the Cub_{bi} / $Ia\bar{3}d$ phase formed by these two compounds. The colours mark clearly the difference of the aromatic/ionic building block self-assembly in the bicontinuous networks. (c) The isoelectron surface in milky enclose the highest 10% unit cell volume, showing the triangular-like junctions of the bicontinuous networks.

Furthermore, to help understand the molecular arrangement in the Cub_{bi} / $Ia\bar{3}d$ phase, its structural data is calculated and summarised in **Table S6**.

Table S6. Structural data of the Cub_{bi} / $Ia\bar{3}d$ phase

Compound	a_{cub}/nm	V_{cell}/nm^3	V_{mol}/nm^3	n_{cell}	L_{net}/nm	n_{raft}
[H-Im][TFSI]	8.5	614	2.4	256	72.1	2.0
[Et-Im][TFSI]	8.7	659	2.5	264	73.8	2.0

[a] Abbreviations: $V_{cell} = a_{cub}^3$, is the volume of the unit cell; V_{mol} is the molecular volume calculated according to the crystal volume increments method by Immirzi;[S1] $n_{cell} = V_{cell} / V_{mol}$, is the molecular number in an unit cell; $L_{net} = 8.485a_{cub}$, is the total length of networks in an unit cell; $n_{raft} = n_{cell} / (L_{net}/h)$, is the molecular number in each h thick raft of the networks, h is the thickness of each molecular raft, here is estimated to be 0.56 nm as to have an integer number of molecules in each raft, e.g., here $n_{raft} = 2$; this is also coherent with the fact that TFSI anion would have an expanding effect on the normal $\pi - \pi$ stacking distance (~ 0.45 nm).

In a brief summary, Cub_{bi} / $Ia\bar{3}d$ phase is observed in both compounds, whereas Col_h phase is only observed in **[H-Im][TFSI]**. The number of molecule in each raft in the networks of Cub_{bi} / $Ia\bar{3}d$ phase is estimated to be 2 for these two compounds; while the number is enlarged to 3 in each raft in the columns of Col_h phase formed in **[H-Im][TFSI]** compound.

10. Ionic conductivity of [H-Im][TFSI] and [Et-Im][TFSI]

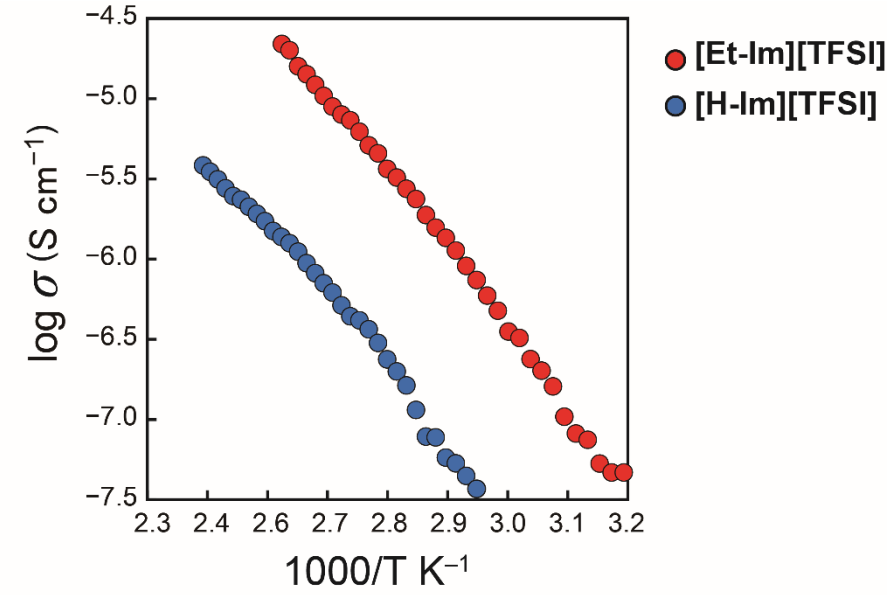

Figure S22. Ionic conductivity of **[H-Im][TFSI]** and **[Et-Im][TFSI]**.

11. Synthesis of [H-Im-diene][TFSI] and [H-Im-diene][FSI]

Scheme S3. Synthesis of [H-Im-diene][TFSI] and [H-Im-diene][FSI].

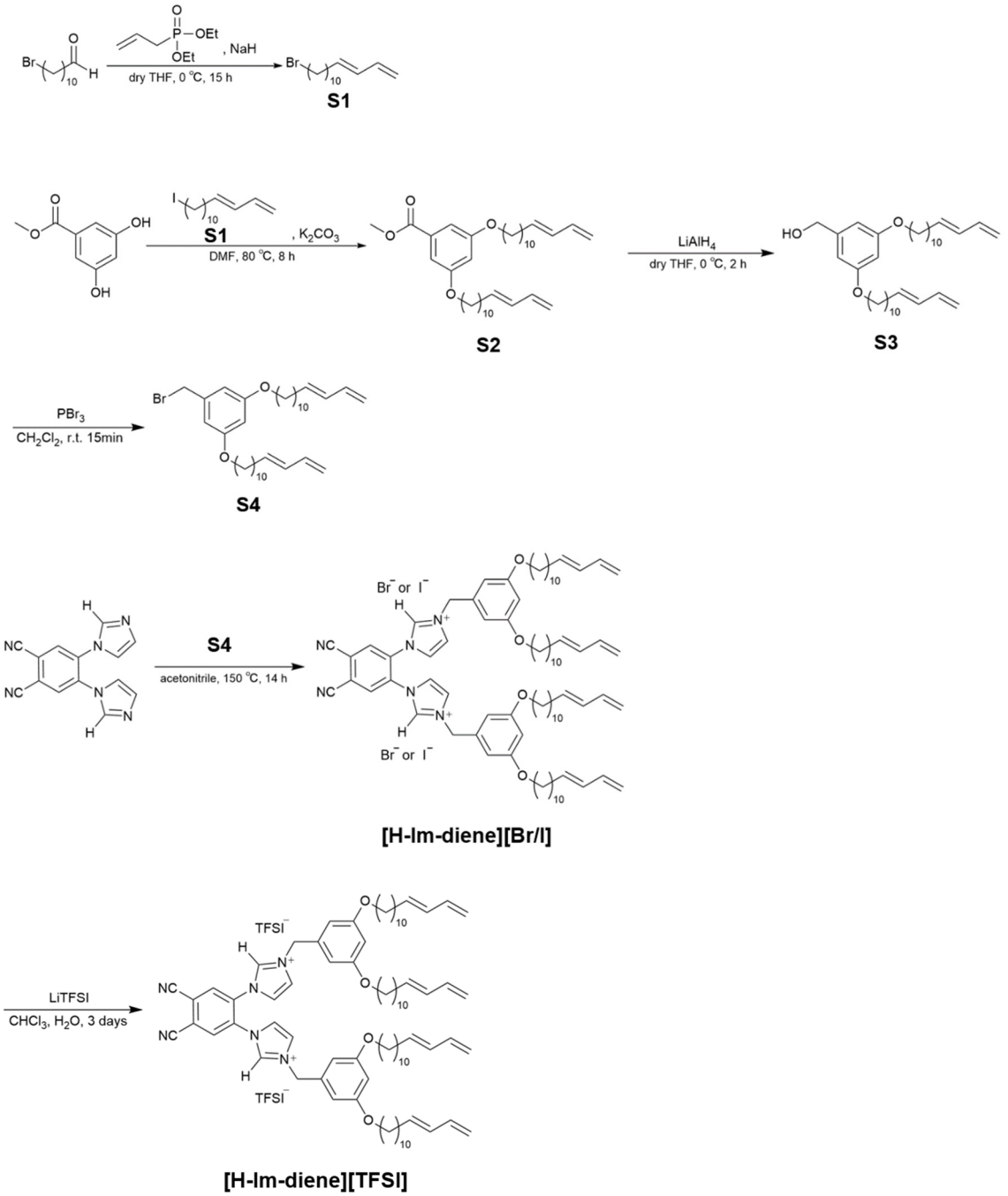

To confirm the hypothesis that the present molecular design can be utilized for the development of CO_2 separation membranes with specific CO_2 transportation pathways, we designed LC monomers analogous to **[H-Im][FSI]** by introducing polymerisable 1,3-diene groups (see **Scheme S3**). Although the synthesis was successful, the small amount of monomer obtained prevented characterisation and evaluations of potential utility. We expect that the molecular design presented herein will contribute to the development of new methods for fabricating next-generation gas-separation membranes.

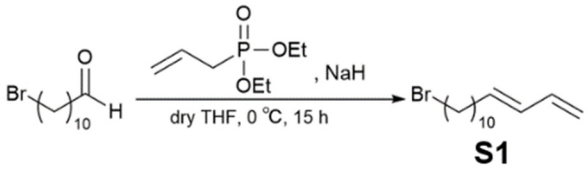

S1

To a stirred suspension of NaH (0.14g, 6.0 mmol) in THF was added a solution of diethyl allylphosphonate (1.0 mL, 6.0 mmol) in dry THF at 0 ℃. To the reaction mixture was added a solution of 1-bromo-undecanaldehyde (1.49 g, 6.0 mmol) dropwisely, and then stirred for 15h at 0 ℃. After quenching with ethanol, the solvent was removed under vacuum. The crude product was extracted with hexane, washed with water, dried over $MgSO_4$, and concentrated with a rotary evaporator. A colorless oily product of **S1** was obtained by column chromatography (eluent: hexane). (yield = 0.379 g, 23%) ^{1}H-NMR (400MHz, $CDCl_3$) δ = 6.35-6.26 (m, 1H), 6.13-5.96 (m, 1H), 5.78-5.66 (m, 1H), 5.08 (d, J = 16.9 Hz, 1H), 4.95-4.85 (m, 1H), 3.46-3.29 (m, 2H), 2.07 (q, J = 7.0 Hz, 2H), 1.92-1.72 (m, 2H), 1.41-1.27 (m, 14H).

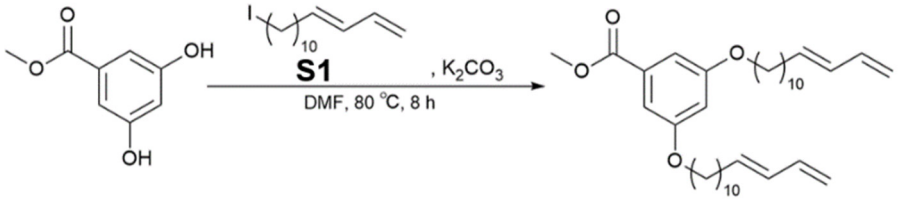

S2

A DMF (5 ml) suspension of methyl 3,5-dihydroxybenzoate (0.060 g, 0.37 mmol), **S1** (0.25 g, 0.92 mmol), and K_2CO_3 (0.31 g, 2.23 mmol) in a round-bottomed flask equipped with a stirring bar was deaerated under reduced pressure, and the flask was filled with argon. After the resulting mixture was heated at 80 °C for 8 h with vigorous stirring, the mixture was poured into a mixture of ethyl acetate, hexane and water. The reaction mixture was extracted three times with ethyl acetate. The organic phase was dried over

anhydrous $MgSO_4$, filtered, and concentrated under reduced pressure. The residue was recrystallized from ethanol to afford **S2** as a white powder (yield = 0.176 g, 89%).
^{1}H-NMR (400 MHz, $CDCl_3$): δ = 7.14 (d, J = 2.8Hz, 2H), 6.62 (t, J = 2.4 Hz, 1H), 6.35-6.25 (m, 2H), 6.07-6.01 (m, 2H), 5.73-5.66 (m, 2H), 5.07 (d, J = 17.2 Hz, 2H), 4.93 (d, J = 10.0 Hz, 2H), 3.95 (t, J = 6.4 Hz, 4H), 3.89 (s, 3H), 2.09-2.04 (m, 4H), 1.80-1.73(m, 4H), 1.47- 1.25 (m, 28H)

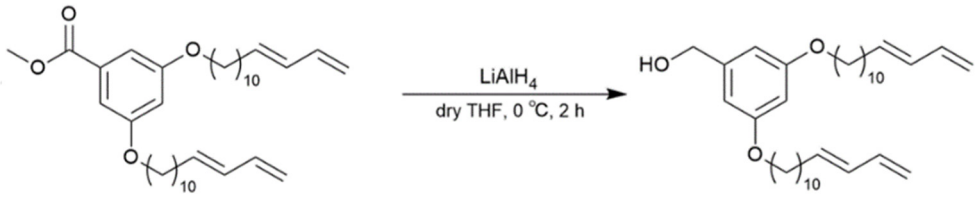

S2 **S3**

To a stirred suspension of $LiAlH_4$ (0.01 g, 0.29 mmol) in dried THF (0.5 mL) was added a solution of **S2** (0.11 g, 0.19 mmol) in THF (5 mL) at 0 ℃ for 2 h. Then the mixture was dried over $MgSO_4$. The insoluble materials were filtered off through filter paper. The filtrate was concentrated by rotary evaporation. The residue was recrystallized from methanol to afford **S3** as a white powder (yield = 0.0595 g, 57%).
^{1}H-NMR (400MHz, $CDCl_3$): δ = 6.50 (s, 2H), 6.38 (t, J = 2.0Hz, 1H), 6.36-6.26 (m, 2H), 6.08-6.01 (m, 2H), 5.74-5.67 (m, 2H), 5.08 (d, J = 16.8Hz, 2H), 4.94 (d, J = 14Hz, 2H), 4.61 (d, J = 6.0Hz, 2H), 3.93 (t, J = 6.8Hz, 4H), 2.10-2.05 (m, 4H), 1.80-1.72 (m, 4H), 1.61 (t, J = 6.0Hz, 1H), 1.47-1.23 (m, 28H).

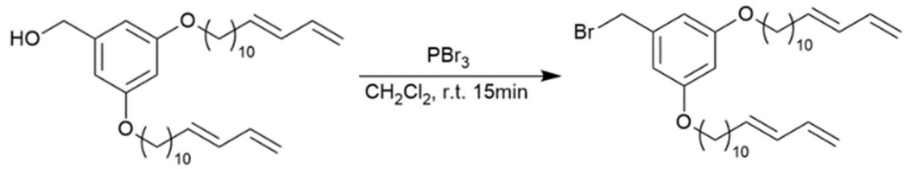

S3 **S4**

To a solution of **S3** (0.0300 g, 0.057 mmol) in CH_2Cl_2 (5 ml) under argon was added dropwise PBr_3 (0.008 mL, 0.085 mmol) with stirring at room temperature. The mixture was stirred at room temperature for 15 min and slowly quenched with hexane, methanol, and water, successively. The reaction mixture was extracted with ethyl acetate and hexane three times. The resulting organic phase was dried over anhydrous $MgSO_4$, filtered, and concentrated under reduced pressure, which afforded **S4** as a solid (yield = 0.0286 g, 85%).

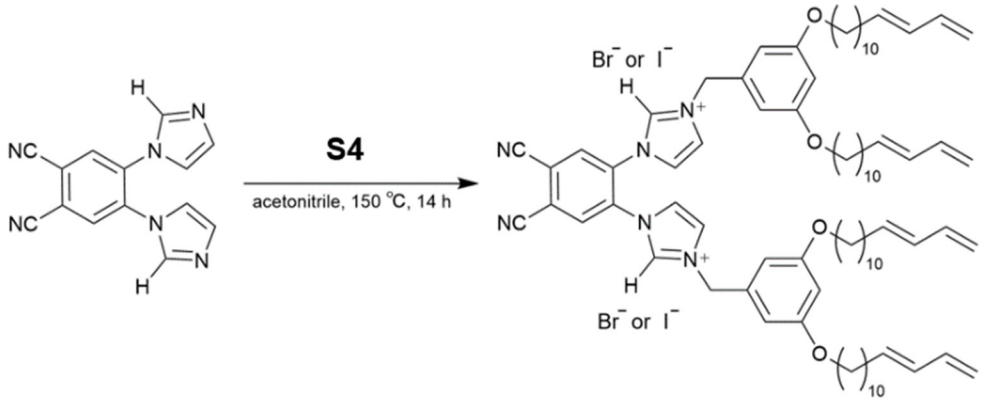

[H-Im-diene][Br/I]

[Him-diene][Br/I]. An acetonitrile (3.0 ml) solution of **S4** (0.13 g, 0.22 mmol), **Head-H** (0.010 g, 0.037 mmol), and NaI (0.10 g, 0.67mmol) in a pressure tube equipped with a stirring bar was heated at 150 °C for 14 h with vigorous stirring. The reaction mixture was extracted three times with $CHCl_3$. The organic phase was dried over anhydrous $MgSO_4$, filtered, and concentrated under reduced pressure to afford **[Him-diene][Br/I]** as a solid. ^{1}H-NMR (400MHz, DMSO-d_6): δ = 9.67 (s, 2H), 8.87 (s. 2H), 7.90 (s, 2H), 7.83 (s, 2H), 6.57 (d, J = 1.8Hz, 4H), 6.52 (s, 2H), 6.31-6.27 (m, 4H), 6.06-5.95 (m, 4H), 5.71 (m, 4H), 5.34 (s, 4H), 5.08 (d, J = 16.9Hz, 4H), 4.95 (d, J = 10.5Hz, 4H), 3.92 (t, J = 6.4Hz, 8H), 2.02-1.96 (m, 8H), 1.69-1.65 (m, 8H), 1.36-1.24 (m, 56H).

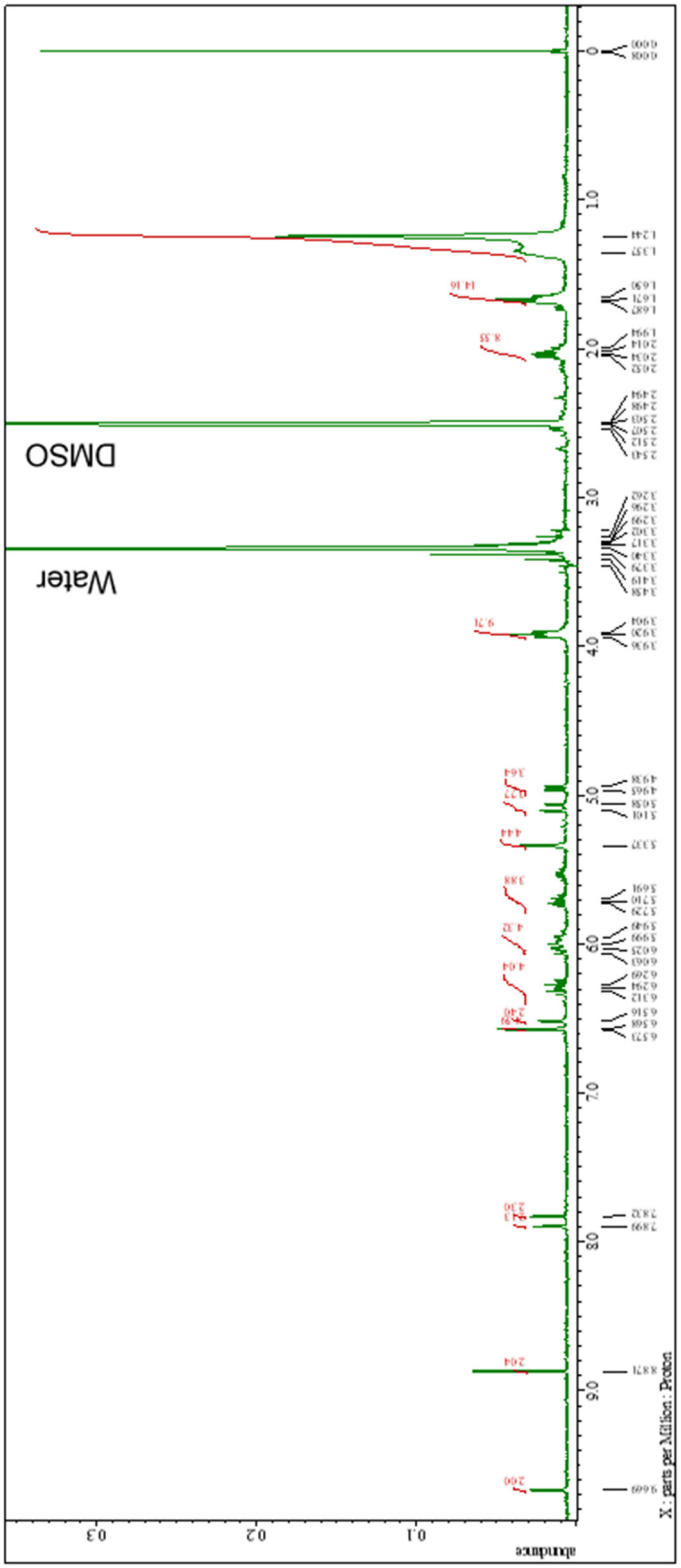

Figure S23. ^{1}H-NMR spectrum of **[H-Im-diene][Br/I]** in DMSO-d_6.

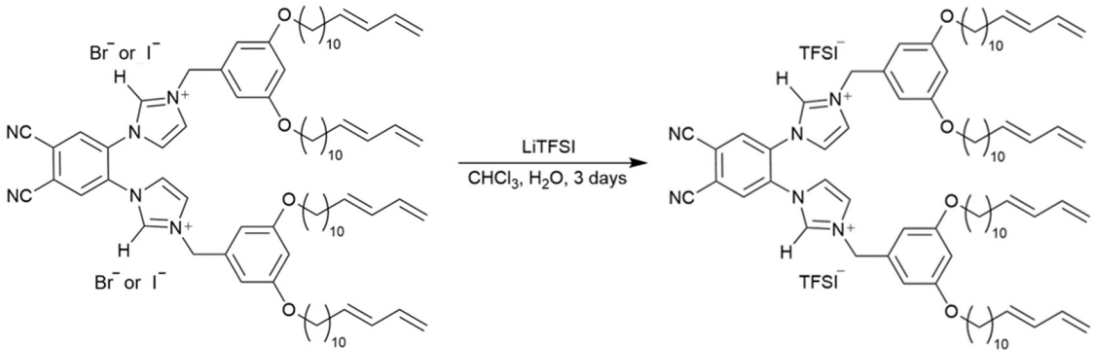

[H-Im-diene][Br/I] **[H-Im-diene][TFSI]**

[H-Im-diene][TFSI]. To a solution of **[H-Im-diene][Br/I]** (0.014g, 0.0098 mmol) in $CHCl_3$ /methanol was added a solution of LiTFSI (0.288 g, 1.00 mmol) in MeOH/water with vigorous stirring at room temperature. The mixture was stirred at room temperature for 12 h. The reaction mixture was extracted with $CHCl_3$ three times. The resulting organic phase was dried over anhydrous $MgSO_4$, filtered, and concentrated under reduced pressure. The crude product was dissolved in $CHCl_3$ and purified by column chromatography on silica gel (eluent: $CHCl_3$/MeOH = 10/1) to afford **[Hi-Im-diene][TFSI]** as a solid.^{1}H-NMR (400MHz, DMSO-d_6): δ = 9.63 (s, 2H), 8.87 (s. 2H), 7.86 (s, 2H), 7.80 (s, 2H), 6.53 (d, J = 1.6 Hz, 4H), 6.48 (s, 2H), 6.28-6.23 (m, 4H), 6.03-5.91 (m, 4H), 5.69-5.65 (m, 4H), 5.30 (s, 4H), 5.04 (d, J = 16.8 Hz, 4H), 4.91 (d, J = 10.8 Hz, 4H), 3.88 (t, 8H), 2.02-1.96 (m, 8H), 1.66-1.21 (m, 64H).

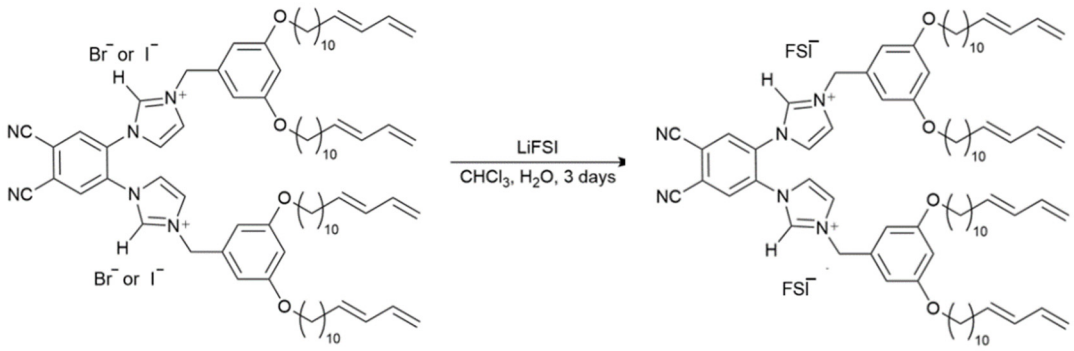

[H-Im-diene][FSI]. To a solution of **[H-Im-diene][Br]** (0.014g, 0.0098 mmol) in $CHCl_3$ /methanol was added a solution of LiFSI (0.187 g, 1.00 mmol) in MeOH/water with vigorous stirring at room temperature. The mixture was stirred at room temperature for 12 h. The reaction mixture was extracted with $CHCl_3$ three times. The resulting organic phase was dried over anhydrous $MgSO_4$, filtered, and concentrated under reduced pressure. The crude product was dissolved in $CHCl_3$ and purified by column chromatography on silica gel (eluent: $CHCl_3$/MeOH = 10/1) to afford **[Hi-Im-diene][TFSI]** as a solid.^{1}H-NMR (400MHz, DMSO-d_6): δ = 9.63 (s, 2H), 8.87 (s. 2H), 7.86 (s, 2H), 7.80 (s, 2H), 6.53 (d, J = 1.6Hz, 4H), 6.48 (s, 2H), 6.28-6.23 (m, 4H), 6.03-5.91 (m, 4H), 5.69-5.65 (m, 4H), 5.30 (s, 4H), 5.04 (d, J = 16.8 Hz, 4H), 4.91 (d, J = 10.8 Hz, 4H), 3.88 (t, 8H), 2.02-1.96 (m, 8H), 1.66-1.21 (m, 64H).

12. Thermal phase transition behavior of [H-Im-diene][X]

12. 1. Thermal phase transition behavior of [H-Im-diene][TFSI]

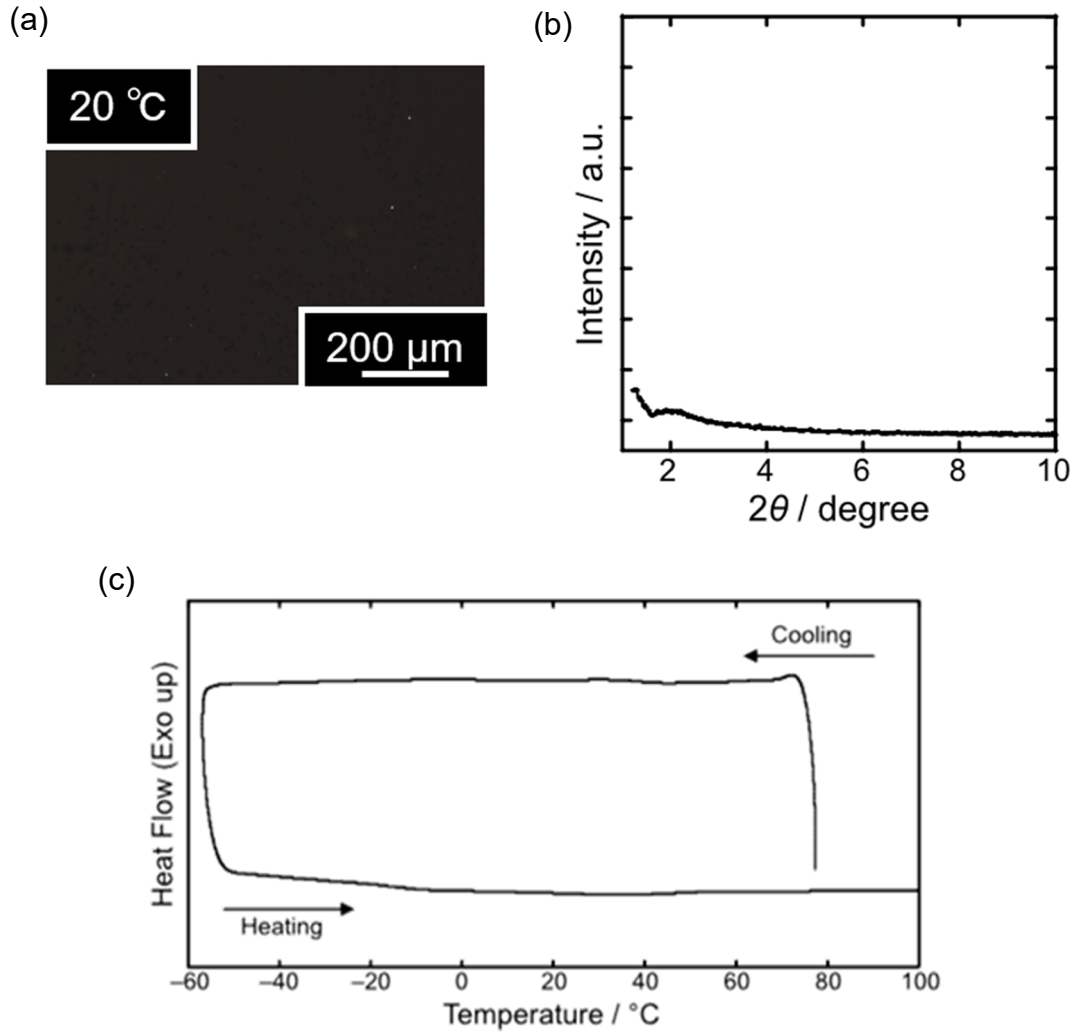

Figure S24. (a) Polarized optical microscopy image of **[H-Im-diene][TFSI]** at 20 °C (b) XRD pattern of **[H-Im-diene][TFSI]** at 25 °C. (c) DSC thermograms of **[H-Im-diene][TFSI]**.

This compound shows no birefringence, which indicates that it forms an isotropic liquid or a cubic phase. The XRD pattern shows negligible diffraction peak. There is no exothermic/endothermic peak corresponding to the formation of mesophases. Based on these results, we conclude that **[H-Im-diene][TFSI]** shows no mesomorphic behaviour.

12. 2. Thermal phase transition behavior of [H-Im-diene][FSI]

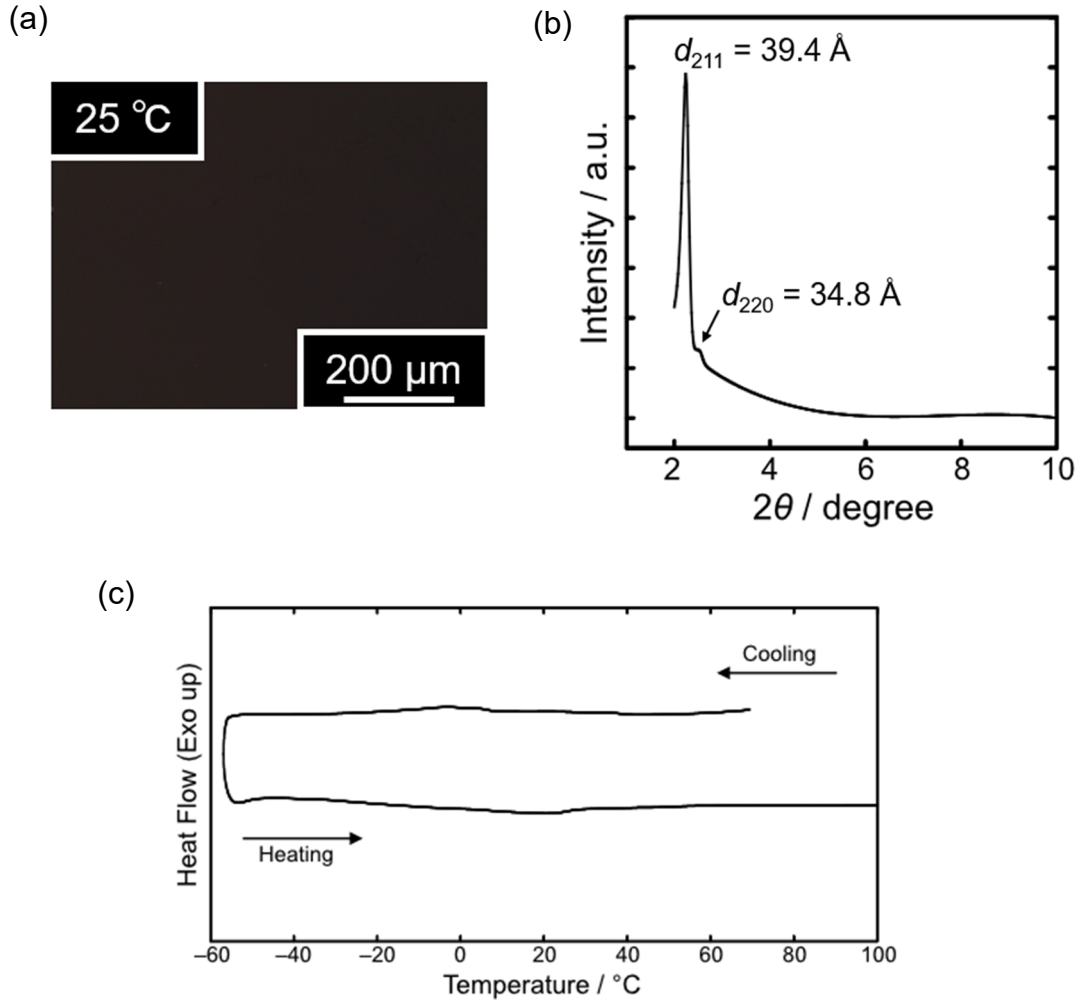

Figure S25. (a) Polarized optical microscopy image of **[H-Im-diene][FSI]** at 25 °C (b) XRD pattern of **[H-Im-diene][FSI]** at 25 °C. (c) DSC thermograms of **[H-Im-diene][FSI]**.

This compound shows no birefringence, which indicates that it forms an isotropic liquid or a cubic phase. The XRD pattern shows two intense peaks that can be assigned to (211) and (220) reflections. Based on these results, we assume that **[H-Im-diene][FSI]** forms a Cub_{bi} phase as well as analogous compounds with no polymerizable groups. Since, in the DSC thermograms, the exothermic/endothermic peaks appear as broad peak, it was difficult to confirm the temperature range forming the mesophase.

Comparing the mesomorphic behaviour of these compounds with polymerizable groups and those of analogous compounds having no polymerizable groups, we have found a trend that the introduction of the polymerizable groups largely lowers the isotropization temperatures. It is a general trend reported for the design of liquid-crystalline monomers.[S2-S5] The isotropization temperature of **[H-Im][FSI]** is about 50 °C higher than that of **[H-Im][TFSI]**, which is attributed to the difference in the anion size. We expect that this difference leads to the presence/absence of the mesomorphic properties after the introduction of the polymerizable 1,3-diene groups.

13. Structures of Stable Conformers

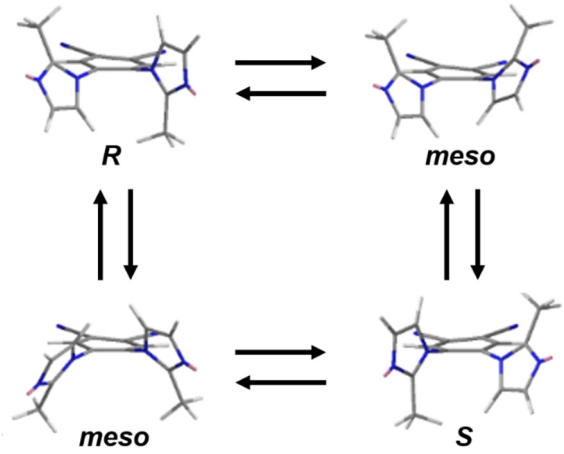

Figure S26. Four stable conformers of 1,2-dicyanobenzene having two 2-methyl-1-imidazolyl moieties. They correspond to the *meso*, *R*, and *S* conformers, respectively.

14. References

S1) A. Immirzi and B. Perini, *Acta Cryst.*, 1977, **A33**, 216–218.

S2) B. P. Hoag and D. L. Gin, *Macromolecules*, 2000, **33**, 8549–8558.

S3) B. A. Pindzola, J. Jin and D. L. Gin, *J. Am. Chem. Soc.*, 2003, **125**, 2940–2949.

S4) M. Yoshio, T. Kagata, K. Hoshino, T. Mukai, H. Ohno and T. Kato, *J. Am. Chem. Soc.*, 2006, **128**, 5570–5577.

S5) T. Ichikawa, M. Yoshio, A. Hamasaki, J. Kagimoto, H. Ohno and T. Kato, *J. Am. Chem. Soc.,* 2011, **133**, 2163–2169.